Acta Neuropathologica (2019) 137:413–436
https://doi.org/10.1007/s00401-019-01965-6

ORIGINAL PAPER

Frontal cortex and striatal cellular and molecular pathobiology in individuals with Down syndrome with and without dementia

Sylvia E. Perez[1,2] · Jennifer C. Miguel[1] · Bin He[1] · Michael Malek-Ahmadi[3] · Eric E. Abrahamson[4,5] · Milos D. Ikonomovic[4,5] · Ira Lott[6] · Eric Doran[6] · Melissa J. Alldred[7,8] · Stephen D. Ginsberg[7,8,9] · Elliott J. Mufson[1]

Received: 28 November 2018 / Revised: 18 January 2019 / Accepted: 22 January 2019 / Published online: 7 February 2019

Abstract

Although, by age 40, individuals with Down syndrome (DS) develop amyloid-β (Aβ) plaques and tau-containing neurofibrillary tangles (NFTs) linked to cognitive impairment in Alzheimer's disease (AD), not all people with DS develop dementia. Whether Aβ plaques and NFTs are associated with individuals with DS with (DSD+) and without dementia (DSD−) is under-investigated. Here, we applied quantitative immunocytochemistry and fluorescent procedures to characterize NFT pathology using antibodies specific for tau phosphorylation (pS422, AT8), truncation (TauC3, MN423), and conformational (Alz50, MC1) epitopes, as well as Aβ and its precursor protein (APP) to frontal cortex (FC) and striatal tissue from DSD+ to DSD− cases. Expression profiling of single pS422 labeled FC layer V and VI neurons was also determined using laser capture microdissection and custom-designed microarray analysis. Analysis revealed that cortical and striatal Aβ plaque burdens were similar in DSD+ and DSD− cases. In both groups, most FC plaques were neuritic, while striatal plaques were diffuse. By contrast, FC AT8-positive NFTs and neuropil thread densities were significantly greater in DSD+ compared to DSD−, while striatal NFT densities were similar between groups. FC pS422-positive and TauC3 NFT densities were significantly greater than Alz50-labeled NFTs in DSD+, but not DSD− cases. Putaminal, but not caudate pS422-positive NFT density, was significantly greater than TauC3-positive NFTs. In the FC, AT8 + pS422 + Alz50, TauC3 + pS422 + Alz50, pS422 + Alz50, and TauC3 + pS422 positive NFTs were more frequent in DSD+ compared to DSD- cases. Single gene-array profiling of FC pS422 positive neurons revealed downregulation of 63 of a total of 864 transcripts related to Aβ/tau biology, glutamatergic, cholinergic, and monoaminergic metabolism, intracellular signaling, cell homeostasis, and cell death in DSD+ compared DSD− cases. These observations suggest that abnormal tau aggregation plays a critical role in the development of dementia in DS.

Keywords Down syndrome · Dementia · Amyloid · Tau · Microarray · Frontal cortex · Striatum

Electronic supplementary material The online version of this article (https://doi.org/10.1007/s00401-019-01965-6) contains supplementary material, which is available to authorized users.

✉ Elliott J. Mufson
elliott.mufson@dignityhealth.org

[1] Department of Neurobiology and Neurology, Barrow Neurological Institute, 350 W. Thomas St, Phoenix, AZ 85013, USA

[2] School of Life Sciences, College of Liberal Arts and Sciences, Arizona State University, Tempe, AZ 85287, USA

[3] Banner Alzheimer's Institute, Phoenix, AZ 85006, USA

[4] Geriatric Research Education and Clinical Center, VA Pittsburgh Healthcare System, Pittsburgh, PA 15213, USA

[5] Departments of Neurology and Psychiatry, University of Pittsburgh, Pittsburgh, PA 15213, USA

[6] Departments of Pediatrics and Neurology, University of California, Irvine, CA 92697, USA

[7] Center for Dementia Research, Nathan Kline Institute, Orangeburg, NY 10962, USA

[8] Departments of Psychiatry, NYU Neuroscience Institute, NYU Langone Medical Center, New York, NY 10021, USA

[9] Departments of Neuroscience and Physiology, The NYU Neuroscience Institute, NYU Langone Medical Center, New York, NY 10021, USA

Introduction

Down syndrome (DS) is a genetic disorder characterized by intellectual disability attributed to a full or partial extra copy of human chromosome 21 (HSA21), that accounts for 95% of the chromosomal anomalies in DS (1% due to mosaicism and 4% due to translocation). In addition, individuals with DS exhibit characteristics of premature aging and are at high risk for developing dementia of the Alzheimer's disease (AD) -type several decades earlier than seen in sporadic AD [118, 137, 138]. By the age of 40, people with DS exhibit β-amyloid (Aβ) senile plaque and tau-containing neurofibrillary tangle (NFT) pathology [135], cholinergic basal forebrain and brainstem monoaminergic cell loss [79, 80, 82, 136], and neurotrophic deficits [52, 53], that may contribute to the early onset of dementia. However, despite consistent and profuse neuropathology, only two-thirds of all adult cases with DS develop dementia [37, 83, 139]. In DS, an increase in soluble Aβ species precedes plaque deposition [42, 121, 127] as early as 21 gestational weeks [42, 121], followed by diffuse deposits of Aβ42 between 8 and 12 years of age, and Aβ40 by the third decade of life, occurring earlier than seen in AD [68, 69, 76]. Positron emission tomography (PET) imaging revealed cortical and subcortical amyloid load visualized by [11C]Pittsburgh compound-B [4, 44, 45, 63], [18F]Florbetapir [84, 112], and [18F]Florbetaben [54] in adult individuals with DS, but differences between DS with (DSD+) and without dementia (DSD-) remain to be clarified. Interestingly, PET imaging found that striatal amyloid precedes that seen in the neocortex [44, 45, 64, 130], which was related to cognitive decline in DS [4]. However, the relation of amyloid pathology to cognition in DSD + and DSD − remains an under-investigated area [46].

Compared to the extensive number of reports of amyloid in the brain of people with DS, the involvement of tau pathology is less well understood. NFT pathology occurs at a later age than Aβ in DS [76, 78, 81, 93], exhibits an age-related pattern similar to AD [47] and, is a better correlate of cognitive decline and dementia in DS [8, 83, 97, 108]. These observations suggest that, despite the appearance of Aβ at an early age, NFT pathology is more closely linked to cognitive decline and dementia in DS. The evolution of NFTs follows a linear progression where tau undergoes posttranslational phosphorylation, conformation, and truncation events in AD [5, 9, 26, 28, 41, 131] where tau phosphorylation occurs early [90, 91] and correlates with AD severity [104, 131]. Despite a single study showing that phosphorylated tau is an early post-transcriptional event in three subjects with DS [92], very little is known about tau posttranslational modifications in NFTs in DSD + and DSD −.

While several cell type specific gene expression profiling studies examined classes of transcripts underlying the molecular pathogenesis of the progression of AD within subcortical [15, 32, 33, 103, 128] and limbic cortical profiles [17, 30], only regional microarray and RNA sequencing (RNA-seq) approaches have been used to detect transcriptional alterations in the human DS brain [39, 73]. To our knowledge, we are not aware of any study that has applied single-cell gene profiling of tau-containing cortical neurons accrued postmortem from individuals with DSD + and DSD −.

The present study examined amyloid plaque and NFT pathology in FC and striatal tissue obtained from subjects who came to autopsy with a clinical diagnosis of DSD + and DSD − using immunohistochemical and histofluorescence approaches combined with quantitative morphometry. In addition, single-population expression profiling of layer V and VI FC neurons immunostained for the phosphorylated pretangle tau maker pS422 was performed in tissue obtained postmortem from the same DS cases − via laser capture microdissection (LCM) coupled with custom-designed microarray analysis [30, 36, 95].

Materials and methods

Subjects

Tissue samples were obtained from a total of 18 individuals with DS (12 DSD + and 6 DSD −) ranging in age from 42 to 60 years obtained from the University of California at Irvine Alzheimer Disease Researcher Center (UCI ADRC; $n = 10$), Rush University Alzheimer's Disease Center (RADC; $n = 7$), and Banner Sun Health Research Institute (BSHRI; $n = 1$) (Table 1). Three RADC, eight UCI ADRC, and one BSHRI DS cases had a clinical diagnosis of AD-like dementia (Table 1). There was no difference in gender frequency, age at death, postmortem interval (PMI), brain weight, or APOE e4 carrier status between the sources of DS tissue (data not shown). DS diagnosis was confirmed by the presence of an extra HSA21 using fluorescence in situ hybridization and/or chromosome karyotyping.

Dementia status of the UCI ADRC and the BSHRI cases was determined in accordance with international classification of diseases and related health problems-tenth revision (ICD-10) and dementia questionnaire for mentally retarded persons (DMR-IV-TR) criteria [124]. All UCI ADRC subjects with DS were followed longitudinally prior to death. Assessments included physical and neurological exams and a history obtained from both the participant and a reliable caregiver. Standardized direct and indirect cognitive and

Table 1 Demographics and neuropathological characteristics of DS cases

Case#	Clinical Diagnosis	Age (y)	Gender	PMI (h)	Brain Weight (g)	APOE	Braak Stage	FC	Str	P-IQ	Source
1	DSD−	42	F	5	1116	3/4	V	✓	–	Moderate	UCI ADRC
2	DSD−	44	F	8	1060	2/3	V	✓	✓	–	RADC
3	DSD−	46	M	3	–	2/3	–	✓	✓	–	RADC
4	DSD−	47	F	5	–	2/3	V	✓	✓	–	RADC
5	DSD−	48	F	18	1093	3/3	III	✓	–	Mild	UCI ADRC
6	DSD−	60	F	15	1030	2/4	V	✓	✓	–	RADC
7	DSD+	45	F	3	944	3/3	VI	✓	–	Moderate	UCI ADRC
8	DSD+	45	F	3	900	3/3	VI	✓	–	Mild	UCI ADRC
9	DSD+	46	M	6	933	2/3	VI	✓	–	Moderate	UCI ADRC
10	DSD+	46	M	20	1090	2/3	VI	✓	✓	–	RADC
11	DSD+	49	M	2	1010	3/3	VI	✓	–	Mild	UCI ADRC
12	DSD+	50	F	5	871	3/4	VI	✓	–	Mild	UCI ADRC
13	DSD+	52	F	4	940	2/3	VI	✓	–	Moderate	UCI ADRC
14	DSD+	55	M	4	823	3/3	VI	✓	–	Moderate	UCI ADRC
15	DSD+	55	M	3	1224	3/3	VI	–	✓	–	BSHRI
16	DSD+	57	F	5	1054	3/3	VI	✓	–	Severe	UCI ADRC
17	DSD+	58	F	12	740	2/3	–	–	✓	–	RADC
18	DSD+	59	F	4	–	2/3	VI	✓	✓	–	RADC

–No available data or tissue

PMI postmortem interval, *FC* frontal cortex, *Str* striatum, *P-IQ* premorbid IQ, *UCI ADRC* University of California at Irvine Alzheimer Disease Researcher Center, *RADC* Rush University Alzheimer's Disease Center, *BSHRI* Banner Sun Health Research Institute

behavioral assessments were also completed. The diagnosis of dementia required deficits in two or more areas of cognitive functioning, and progressive worsening of cognitive performance compared to the individual's baseline performance. Cognitive decline due to confounding factors that may mimic dementia (e.g., depression, sensory deficits, and hypothyroidism) was eliminated. Premorbid intelligence quotient (IQ) was also determined in all UCI ADRC DS cases. Dementia diagnosis for the RADC cases was determined by a neurologist trained in gerontology and in discussion with a caregiver. Human Research Committees of Rush University Medical Center and University of California at Irvine approved this study. Table 1 details the clinical, demographic and neuropathological features and tissue source of the individuals with DSD + and DSD −.

Chromogen-based immunohistochemistry

FC [Brodmann area (BA8) and/or (BA9)] tissue fixed in either 4% paraformaldehyde or 10% formalin from 6 DSD − and 10 DSD + and striatum (caudate and putamen) from 4 DSD − and 4 DSD + cases were cut on a sliding freezing microtome at 40 µm thickness and stored in cryoprotectant at − 20 °C prior to processing [103] (Table 1). FC and striatal sections were processed for single-label avidin–biotin-based immunohistochemistry using the following primary antibodies: rabbit polyclonal anti-phosphorylation pS422 tau, (1:1000, Invitrogen, Carlsbad, CA), mouse monoclonal anti-phosphorylation clone AT8 tau (1:1000, Invitrogen), mouse monoclonal anti-conformation Alz50 (1:1000), and MC1 tau (1:1000, both Gifts from Dr. Peter Davies, Hofstra Northwell School of Medicine, Manhasset, New York), mouse monoclonal anti-truncation TauC3 (1:1000, ThermoFisher, Waltham, MA) and MN423 (1:5000, gift

Table 2 List of antibodies

Antigen	Antibody	Dilution IH (IF)	Company Catalog#
APP/Aβ (6E10)	IgG1 mouse monoclonal to residues 1–16 of Aβ	1:1000	BioLegend #803002
Aβ (MOAB2)	IgG2b mouse monoclonal to Aβ	1:800	Gift from M. J. LaDu
Aβ42	IgG rabbit polyclonal to Aβ42	1:1000	Millipore #AB5078
Conformational Tau (Alz50)	IgM mouse monoclonal to tau residues 5–15, 312–322	1:1000 (1:50)	Gift from P. Davies
Conformational Tau (MC1)	IgG1 mouse monoclonal to tau residues 5–15, 312–322	1:1000	Gift from P. Davies
Phosphorylated Tau (pS422)	IgG rabbit polyclonal to tau phospho-Serine 422	1:1000 (1:50)	Invitrogen # 03151
Phosphorylated Tau (AT8)	IgG1 mouse monoclonal to tau phospo-Serine 202 and phospho-Threonine 205	1:1000 (1:50)	Invitrogen # MN1020
Truncated Tau (TauC3)	IgG1 mouse monoclonal to truncated tau at 421/422 residues	1:1000 (1:50)	ThermoFisher # AHB0061
Truncated Tau (MN423)	IgG1 mouse monoclonal to truncated tau at glutamic acid 391	1:5000	Gift from L. Binder
Choline Acetyltransferase (ChAT)	IgG goat polyclonal to human placental choline acetyltransferase	1:800 (1:50)	Millipore #AB144P
Tyrosine Hydroxylase (TH)	IgG rabbit polyclonal to tyrosine hydroxylase	1:1000	Invitrogen #OPA1-04050
Neurofilament (SMI-34)	IgG1 mouse monoclonal to phosphorylated neurofilament H	1:1000	BioLegend #8535503
Sirtuin 6	IgG rabbit polyclonal to amino acids 330-348 of human Sirt6	1:5000	Sigma #S4197

IH Immunohistochemistry, *IF* Immunofluorescence

from the late Dr. Lester Binder), and monoclonal antibodies against APP/Aβ (6E10; 1:1000, BioLegend, San Diego, CA) and Aβ (MOAB2; 1:800, gift from Dr. Mary Jo LaDu, University of Illinois, Chicago, IL) (Table 2). Sections processed using the MOAB2 antibody were pretreated with formic acid (75%, 5 min). Immunohistochemistry was performed on two to three sections per case/region. Sections were washed in Tris-buffered saline (TBS), incubated in 0.1 M sodium metaperiodate (Sigma, St. Louis, MO) to inactivate endogenous peroxidase, then permeabilized in TBS containing 0.25% Triton-X (ThermoFisher) and blocked in the same solution containing 3% goat serum for 1 h. Sections were then incubated with primary antibodies overnight at room temperature (RT) in 0.25% Triton-X-100 and 1% goat serum solution [103]. The next day, after three TBS washes containing 1% goat serum, sections were incubated with affinity-purified goat anti-rabbit or anti-mouse biotinylated secondary antibodies (1:200 dilution) for 1 h (Vector Labs, Burlingame, CA). Following washes in TBS, sections were incubated in Vectastain ABC kit (Vector Labs) for 1 h and developed in acetate-imidazole buffer containing 0.05% 3,3′-diaminobenzidine tetrahydrochloride (DAB, Sigma, St. Louis, MO). Reaction was terminated in acetate-imidazole buffer, and sections were mounted to charged slides, air-dried, dehydrated, cleared in xylenes, and cover-slipped. At least one section was counter stained with cresyl violet (Sigma) for cytoarchitectural identification. To validate custom-designed microarray expression data, additional FC sections from both groups were incubated with a rabbit polyclonal antibody against the human nuclear sirtuin 6 (SIRT 6; 1:5000, Sigma), after performing antigen retrieval using Dako target retrieval solution, pH 9 (DAKO, Carpinteria, CA) for 20 min in a steamer [96].

To visualize the relationship between amyloid plaques and tau-containing neurites, additional cortical and striatal sections were dual immunolabeled using two different colored chromogens. Mouse monoclonal antibodies directed against MC1 (1:1000) and phosphorylated neurofilament H (SMI-34; 1:1000, BioLegend) labeled tau-containing neurites were treated with a rabbit polyclonal antibody against the C-terminal of Aβ42 (1:1000, Millipore) for plaques [106]. Likewise, additional striatal sections were processed using a goat polyclonal antibody (1:800, Millipore) to label choline acetyltransferase (ChAT) positive interneurons, a rabbit polyclonal antibody to mark tyrosine hydroxylase (TH; 1:800, Invitrogen) profiles, and 6E10 to label APP/Aβ and rabbit Aβ42 to visualize amyloid plaques (Table 2). Following MC1, SMI-34, ChAT, or TH-labeling sections were

incubated in an avidin/biotin blocking kit (Vector Laboratories) and any remaining peroxidase activity was quenched with a solution containing 3% H_2O_2 for 30 min at RT. Blocking buffer was reapplied for 1 h at RT and incubated in the second primary antibody (Aβ42 or 6E10) overnight at RT, followed by the appropriate biotinylated secondary antibody (1:200 in dilution buffer; Vector Labs) for 1 h at RT. The following day sections were incubated in ABC solution as described above. Sections were processed with the Vector SG Substrate Kit (blue reaction product, Vector Laboratories) according to the manufacturer's protocol. This dual staining resulted in an easily identifiable two-colored profile: brown for ChAT, TH, MC1, and SMI-34 positive profiles and dark blue/black for Aβ42 and APP/Aβ positive plaques. Slides were air-dried, dehydrated, cleared in xylenes, and cover-slipped. Omission of primary antibodies resulted in no detectable immunostaining (not shown).

Immunofluorescence

Free-floating sections were triple labeled with pS422 (1:50), AT8 (1:50) and Alz50 (1:50), or pS422, and Alz50 and TauC3 (1:50) antibodies [103]. Immunoglobulin class IgG and IgM antibodies were employed to detect TauC3, AT8, and Alz50, respectively, allowing TauC3 or AT8 to be distinguished from Alz50. Tissue was singly incubated overnight for AT8 or TauC3 followed by pS422 and Alz50 at RT. The appropriate secondary antibody was applied in the following sequence: first, Cy5-conjugated donkey anti-mouse IgG for AT8 or TauC3 (1:200, Jackson Immuno-research, West Grove, PA); second, Cy3-donkey anti-rabbit IgG for pS422 (1:400, Jackson Immuno-research), and thirdly, Cy2-donkey anti-mouse IgM for Alz50 (1:200, Jackson Immuno-Research). Auto-fluorescence was blocked with Auto-fluorescence Eliminator Reagent (Millipore, Burlington, MA) according to the manufacturer's instructions. Sections were mounted to charged slides, air-dried, and cover-slipped with aqueous mounting media (Thermo Scientific). Fluorescence was visualized and photographed with an LSM 710 Zeiss confocal microscope (Zeiss, Germany) equipped with Zen 2009 software using excitation lasers at wavelength 488, 560, and 633 nm to see Cy2 (emission green), Cy3 (emission red; pseudocolored blue), and Cy5 (emission infrared; pseudocolored red) fluorochromes, respectively. To determine the chemical phenotype of striatal NFTs, sections were double immunolabeled for ChAT (1:50) and AT8 (1:50) using secondary antibodies Cy3-donkey anti-goat and Cy2-donkey anti-mouse IgGs [103], respectively. For comparison, striatal sections from a non-cognitively impaired (71-year-old female) and a severe AD (76-year-old female) case were processed as described above. Dual immunofluorescence was visualized with the aid of a Revolve Fluorescent Microscope (Echo laboratories, San Diego, CA) with excitation filters at wavelengths 489 and 555 nm for Cy2 and Cy3, respectively [75].

X-34 and 6-CN-PiB histofluorescence

X-34 and 6-CN-PiB histofluorescence was used to assess amyloid burden in the FC and striatum [105]. Sections were mounted to charged slides, air-dried, and rinsed in potassium phosphate buffered saline (KPBS, 0.076% NaCl, 0.0152% K_2HPO_4, and 0.002% KH_2PO_4, pH 7.4). To reduce autofluorescence prior to X-34 and 6-CN-PiB staining, sections were incubated sequentially in 0.25% $KMnO_4$ for 20 min, twice in KPBS for 2 min, in 1% potassium meta-bisulfite and oxalic acid for 5 min and twice in KPBS for 2 min. Sections were rinsed in KPBS, incubated in 100 µM X-34 for 10 min, dipped in tap water, and incubated in 0.2% NaOH made with 80% EtOH [49] or incubated in 10 µM 6-CN-PiB for 45 min, dipped three times in KPBS followed by a 1-min differentiation in KPBS [50]. Subsequently, sections were rinsed in running tap water for 10 min and cover-slipped with Fluoromount (Electron Microscopy Services, Hatfield, PA). X-34 was visualized using an ultraviolet filter and 6-CN-PiB was visualized using a hydroxycoumarin filter (Chroma, Bellows Falls, VT) using an Olympus BX3 microscope with epifluorescence. X-34 is a highly fluorescent derivative of Congo red, which detects the full spectrum of amyloid deposits: neuritic and diffuse plaques and cerebrovascular amyloid, as well as neurofibrillary pathology [49, 126], while 6-CN-PiB is a highly fluorescent derivative of Pittsburgh Compound-B, which reveals only amyloid deposits [50].

Amyloid plaque load and number

Relative numbers and load of 6E10 and MOAB2 immunoreactive (-ir) plaques were evaluated in two FC sections (five fields per section) at 10× magnification covering an area of 1.10 mm^2/field [104]. Three caudate and five putamen fields per section were analyzed with a 20× objective covering an area of 0.20 mm^2/per field in two striatal sections. Plaque load was determined as percentage area per cortical and striatal field by an investigator blinded to clinical diagnosis, and means were calculated per section. Quantification was performed with the aid of a Nikon Eclipse microscope coupled with NIS-Elements Imaging software (Nikon, Japan).

NFT and neuropil thread (NT) quantitation

Since MC1, Alz50, pS422, TauC3, and AT8-ir tau profiles were consistently observed in FC layers V and VI, which are prone to NFTs [7, 10, 47], the relative numbers of NFTs and NTs positive for these tau markers were evaluated in the FC and striatum. Since MN423-positive tau profiles were inconsistently observed in FC layers V and VI, we also counted

layer III MN423 NFTs. MN423 profiles were absent in the striatum. For each tau marker, NFTs and NTs within the FC were counted in at least two sections within four fields per section using a 20× and 40× objective covering an area of 0.14 and 0.03 mm^2 per field, respectively. Due to the limited number of striatal tau positive NTs, only NFTs were counted in two sections containing the caudate and putamen within three-to-five random fields per section, respectively, using a 10× objective covering an area of 1.10 mm^2 per field. An investigator blinded to clinical diagnosis performed counts and data were presented as mean counts per section.

NFT immunofluorescence counts

Semiquantitative counts of FC sections following triple immunofluorescent straining for AT8, pS422, and Alz50 or TauC3, pS422, and Alz50-positive NFTs in layer V and VI were performed in ten fields in a single section, using a 20× objective covering an area per field of 0.10 mm^2 using a Revolve microscope (Echo Laboratories, San Diego, CA) coupled with appropriate fluorescent filters by an investigator blinded to clinical diagnosis. Mean counts were calculated per section.

Statistical analysis for morphometric analyses

Data derived from counts, demographic, and clinical characteristics between groups were evaluated using Mann–Whitney, Kruskal–Wallis, Fisher's test, Wilcoxon signed-rank, and Friedman repeated-measures test followed by Tukey, Conover–Inman, and Dunn's post hoc test for multiple comparisons as appropriate. Spearman rank sum test was used to evaluate linear associations among the variables (Sigma Plot 14, Systat Software, San Jose, CA). False discovery rate (FDR) was used to correct for multiple comparisons among the correlations. Statistical significance was set at 0.05 (two-tailed) and measurements were graphically represented using Sigma Plot 14.0 software (Systat Software).

Single-population expression profiling

Individual immunolabeled pS422 layer V and VI FC neurons (a total of 60 neurons per case pooled/per assay) from DSD − ($n = 5$) and DSD + ($n = 10$) cases were accrued by LCM (PALM MicroBeam C IP, Carl Zeiss MicroImaging Inc, Thornwood, NY). mRNA amplification was performed using terminal continuation (TC) RNA amplification, which preserves the original quantitative relationships among the transcripts [2, 12, 24, 31]. Microdissected FC neurons were homogenized in Trizol solution (ThermoFisher Scientific), and RNAs were reverse transcribed in the presence of the poly d (*T*) primer (100 ng/ml) and TC primer (100 ng/ml) in 1× first strand buffer (ThermoFisher Scientific), 500 uM dNTPs, 5 mM DTT, 20 U of SuperRNase Inhibitor (ThermoFisher Scientific), and 200 U of reverse transcriptase (ThermoFisher Scientific). Single-stranded cDNAs were digested with RNase H and re-annealed with the primers in a thermal cycler: RNase H digestion step at 37 °C, 30 min; denaturation step 95 °C, 3 min; primer reannealing step 60 °C, 5 min. This step generated cDNAs with double-stranded regions at the primer interface. Samples were then purified by column filtration (Montage PCR filters; Millipore, Billerica, MA). RNA hybridization probes were synthesized by in vitro transcription with the use of ^{33}P incorporation in 40 mmol/L Tris (pH 7.5); 6 mmol/L MgCl2; 10 mmol/L NaCl; 2 mmol/L spermidine; 2.5 mmol/L DTT; 125 µmol/L ATP, GTP, and CTP; 2.5 µmol/L cold UTP; 20 U of RNase inhibitor; 2 kU of T7 RNA polymerase (Illumina, San Diego, CA); 60 µCi of 33P-UTP (PerkinElmer, Waltham, MA). The labeling reaction was performed at 37 °C for 4 h. Radiolabeled terminal continuation RNA probes were hybridized to custom-designed microarrays without further purification. Arrays were run in triplicate for each case.

Custom-designed microarray platforms and data analysis

Platforms consist of 1 µg of linearized cDNA purified from plasmid preparations adhered to high-density nitrocellulose (Hybond XL, GE Healthcare, Piscataway, NJ) [24, 31, 34, 95]. cDNA was verified by sequence analysis and restriction digestion. Approximately 864 cDNAs comprised the custom array platform. Arrays were hybridized for 24 h in a solution consisting of 6× saline-sodium phosphate-ethylenediaminetetraacetic acid (SSPE), 5× Denhardt's solution, 50% formamide, 0.1% sodium dodecyl sulfate (SDS), and denatured salmon sperm DNA (200 µg/ml) at 42 °C in a rotisserie oven. Following the hybridization protocol, arrays were washed sequentially in 2× SSC/0.1% SDS, 1× SSC/0.1% SDS and 0.5× SSC/0.1% SDS for 15 min each at 37 °C. Arrays were placed in a phosphor screen for 24 h and developed on a phosphor imager (Storm 840, GE Healthcare, Piscataway, NJ).

Hybridization signal intensity was determined utilizing ImageQuant software (GE Healthcare). Briefly, each array was compared to negative control arrays utilizing the respective protocols without any starting RNA. Expression of TC amplified RNA bound to each target minus background was then expressed as a ratio of the total hybridization signal intensity of the array (a global normalization approach). Global normalization effectively minimizes variation due to differences in the specific activity of the synthesized probe and the absolute quantity of probe [32].

Relative changes in total hybridization signal intensity and individual mRNAs between groups were analyzed using the Mann–Whitney Rank sum test. Adjustment for multiple comparisons was applied within each group of genes using false discovery rates. Expression levels were analyzed and clustered using bioinformatic and graphic software packages (GeneLinker Gold, Improved Outcomes Inc., Kingston, ON). Level of statistical significance was set at $p \leq 0.05$.

Results

Demographics

There was no difference in gender, age at death, postmortem interval (PMI), brain weight, or APOE e4 carrier status when comparing DSD + and DSD − ($p > 0.05$) (Table 3). Braak NFT scores were significantly higher in DSD + cases compared to DSD − cases ($p < 0.001$) (Table 3). All DSD + cases had a Braak score of VI, while 4/5 DSD − cases had a Braak score of V (Tables 1 and 3). Fifty percent of UCI ADRC cases showed a moderate IQ, 40% a mild and 10% showed a severe premorbid IQ. These data were not available for RADC cases (see Tables 1 and 3).

Cortical and striatal plaque load and numbers in DSD − and DSD+

FC and striatal plaque load and number were determined in DSD + and DSD − sections immunolabeled with 6E10 and MOAB2 antibodies (Fig. 1). Histofluorescence compounds X-34 and 6-CN-PiB were also used to determine amyloid load (Fig. 2). FC plaques appeared round with well-defined borders (Figs. 1a–d and 2a–d), while striatal plaques were diffuse and lacked well-defined limits (Figs. 1e–l and 2e–h).

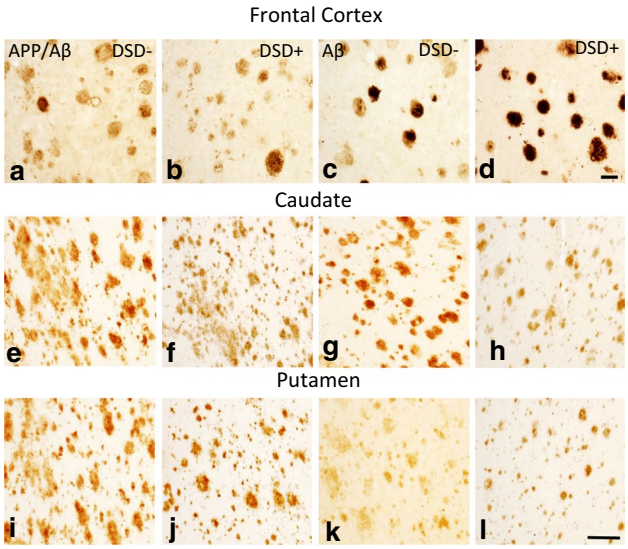

Fig. 1 Photomicrographs showing frontal cortex (FC) APP/Aβ (6E10) (**a**, **b**) and Aβ (MOAB2) (**c**, **d**) immunoreactive (-ir) plaques in 46-year-old male non-demented (**a**, **c**) and 46-year-old male demented (**b**, **d**) subjects with DS. Note the rounded shape of the plaques in both cases. Photomicrographs of APP/Aβ (6E10) (**e, f, i, j**) and Aβ (MOAB2)-ir (**g, h, k, l**) plaques in the caudate (**e–h**) and in the putamen (**i–l**) in a 47-year-old female non-demented and a 46-year-old male demented individual with DS. Note the "amorphous" shape of the APP/Aβ and Aβ-ir plaques in both cases and the greater abundance of APP/Aβ-ir (**e, i**) compared to Aβ-ir plaques (**g, k**) in the caudate and putamen of the non-demented individual with DS. 50 µm scale bar in **d** and **l** applies to **a–c** and **e–h**, **i–k**, respectively

FC immunohistochemical and histofluorescent positive Aβ plaques were detected in all cases. Statistical analyses

Table 3 Summary of the demographics and neuropathology of DS cases

	DSD- ($n=6$)	DSD+ ($n=12$)	p value	Group-wise comparisons
Age (years) [range]	47.80 ± 6.30* [42, 60]	51.40 ± 5.20 [45, 59]	0.24[a]	–
Male/female	1/5	5/7	0.60[b]	–
PMI (h) [range]	9.00 ± 6.00 [18.50, 3.00]	5.90 ± 5.10 [20.00, 2.20]	0.18[a]	–
Brain weight (g) [range]	1074.75 ± 37.70 [1116, 1030]	957.10 ± 133.30 [1224, 740]	0.06[a]	–
APOE e4 (n)	2	1	0.25[b]	–
Braak Scores (n)	III (1), V (4)	VI (11)	0.001[a]	DSD − < DSD +

1 DSD- and 1DSD + subjects do not have Braak scores

2 DSD- and 1 DSD + subjects do not have brain weight

*Mean ± standard deviation

[a]Mann–Whitney rank sum test

[b]Fisher's exact test

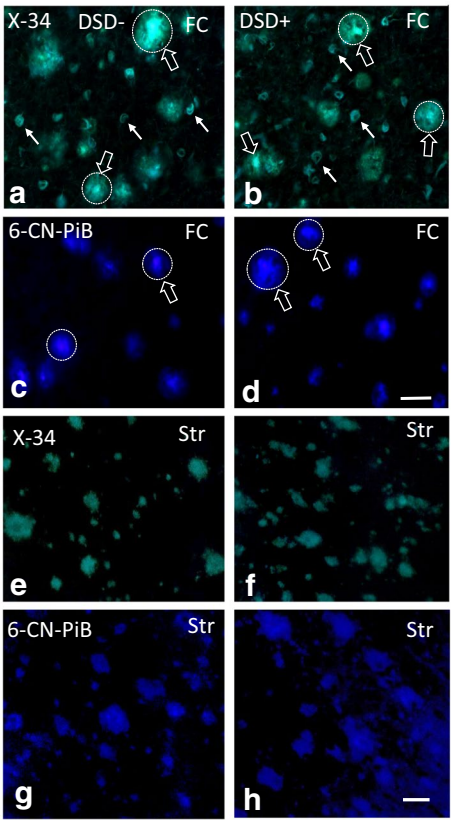

Fig. 2 Photomicrographs of frontal cortex X-34 (**a**, **b**) positive plaques (unfilled white arrows) and NFTs (filled white arrows) and 6-CN-PiB (**c, d**) positive plaques (unfilled white arrows) in a 44-year-old female non-demented (**a, c**) and a 59-year-old female demented (**b, d**) subject with DS. Note the intense fluorescence for both dyes (unfilled arrows) in the center of the plaques (dotted circles), characteristic of classic cored/neuritic plaques. Images showing X-34 (**e**, **f**) and 6-CN-PiB (**g**, **h**)-positive plaques in the caudate of a 46-year-old male non-demented and a 59-year-old female demented DS case. Note the diffuse, less intense pattern of X-34 and 6-CN-PiB histofluorescence and the lack of a center core compared to FC plaques (**a**–**d**). Abbreviations: FC, frontal cortex, Str, striatum. 50 μm scale bar in **d** and **h** applies to **a**-**c** and **e**-**g**, respectively

revealed no significant differences in cortical APP/Aβ, Aβ, X-34 and 6-CN-PiB plaque loads between DS groups (Online Resource 1a, b, Mann–Whitney rank sum test, APP/Aβ $p=0.30$, Aβ $p=0.50$, X-34 $p=0.14$, 6-CN-PiB $p=0.30$). In addition, APP/Aβ and Aβ-ir plaque numbers were statistically comparable between groups (Online Resource 1c, Mann–Whitney rank sum test: APP/Aβ $p=0.74$, Aβ $p=0.55$). By contrast, cortical APP/Aβ and X-34 plaque load was significantly higher than Aβ (Online Resource 1a, Mann–Whitney rank sum test, $p=0.031$) and 6-CN-PiB (Online Resource 1c, Mann–Whitney rank sum test, $p=0.004$) plaque load, respectively, in DSD+, while cortical APP/Aβ and Aβ plaque numbers were similar in both groups (Online Resource 1c, DSD-, Mann–Whitney rank sum test, $p=0.11$ and DSD+, Mann–Whitney rank sum test, $p=0.50$).

Striatal APP/Aβ, Aβ, X-34, and 6-CN-PiB-positive plaques were observed in all cases (Figs. 1 and 2) with the exception of DSD+case 15 (see Table 1), where Aβ-ir plaques were not detected. Statistical analyses revealed no significant differences in caudate or putamen APP/Aβ, Aβ, X-34 and 6-CN-PiB plaque load and APP/Aβ, Aβ plaque numbers between DSD+($n=4$) and DSD− ($n=4$) groups (Online Resource 2, Mann–Whitney rank sum test, $p>0.05$). However, while caudate and putamen APP/Aβ and X-34 load displayed higher mean values than Aβ and 6-CN-PiB in DSD- compared to DSD+(Online Resource 2a, b), only APP/Aβ plaque number in the striatum was significantly increased compared to Aβ plaque number in DSD− (Fig. 1e–l and Online Resource 2c, Mann–Whitney rank sum test, $p<0.029$), but not in DSD+.

FC and striatal X-34, and 6-CN-PiB profiles in DSD- and DSD+

X-34, and 6-CN-PiB staining, which reveal β-pleated sheet structures, was performed to establish the extent of fibrillar Aβ (conformational state) deposits in FC and striatum in both DS groups (Fig. 2). FC plaques were strongly reactive with the pan-amyloid X-34 and fibrillar Aβ selective 6-CN-PiB markers in both DS groups (Fig. 2a–d), while weaker reactivity was observed for plaques stained within either marker in the striatum (Fig. 2e–f). Many cortical X-34 and 6-CN-PiB positive plaques displayed a stronger central than peripheral reactivity (Fig. 2a–d), consistent with classic cored plaques. In addition, X-34 revealed NFTs and NTs in the FC (Fig. 2a, b), but not in the striatum (Fig. 2e, f), in both DS groups, indicating that at the age range examined the majority of FC plaques consisted of dense fibrillar deposits with a β-pleated sheet conformation, a feature of neuritic/compact plaques, whereas less fibrillar Aβ was seen in diffuse plaques, the main striatal plaque component.

Dystrophic neurites surround cortical but not striatal plaques in DSD − and DSD+

To evaluate whether FC and striatal plaques were associated with dystrophic neurites, sections were double labeled with 6E10 or Aβ42 antibodies and SMI-34, MC1, ChAT, or TH. Cortical MC1-positive dystrophic neurites were observed in all cases examined and virtually all FC plaques displayed numerous swollen MC1 and SMI-34 positive dystrophic neurites in both DS groups (Fig. 3a–h). In addition, MC1 and SMI-34-ir NFT and NT profiles were observed in FC in both DSD− and DSD+cases (Fig. 3a, d, f). By contrast MC1, SMI-34, ChAT, and TH-ir dystrophic neurites and NTs were not detected in the striatum in either DS group

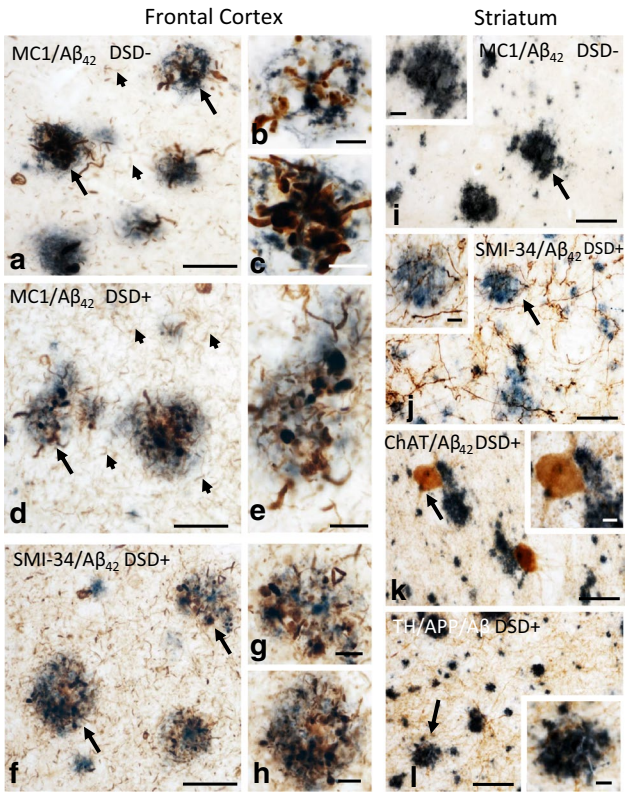

Fig. 3 Photomicrographs of dual-labeled frontal cortex sections showing dystrophic neurites displaying immunoreactivity for the tau conformational epitope MC1 (brown) intermingled within Aβ42-ir plaques (blue) in a 47-year-old female non-demented (**a**) and a 46-year-old male demented (**d**) individual with DS. Note the presence of numerous MC1-ir NTs (small arrows) in the demented compared to non-demented DS case. **b**, **c** and **e**, High-power images of plaques (large arrows in **a** and **d**) displaying dystrophic neurites. Images of frontal cortex showing Aβ42-ir plaques (blue) surrounded by dystrophic neurites positive for the phosphorylated neurofilament H marker SMI-34 (dark brown) in a 46-year-old male demented person with DS (**f**). **g** and **h**, High-power images showing the bulbous nature of the dystrophic neurites within Aβ42-ir plaques shown in **f** (arrows). Photomicrographs of the putamen showing Aβ42-ir plaques (dark blue) and neuropil lacking MC1-ir dystrophic neurites (brown) in a 47-year-old female non-demented individual with DS (**i**). Inset shows high-power image of Aβ42-ir plaque from **i** (arrow). **j**, Image of a dual-labeled caudate section demonstrating the absence of SMI-34-ir (dark brown) dystrophic neurites within Aβ42-ir plaques (blue) in a 46-year-old male demented subject with DS. Inset show an apparent intact SMI-34-ir fibers (arrow) in close proximity to an Aβ42-ir plaque (**j**). **k** and **l** Images showing Aβ42-ir plaques (dark blue) and ChAT-ir neurons (brown) (**k**) as well as APP/Aβ-ir plaques (blue) and TH-ir fibers (brown) (**l**) in the putamen of a 46-year-old male demented subject with DS. Note the lack of ChAT-ir (**k**) and TH-ir (**l**) dystrophic neurites within plaques. Insets in **k** and **l** images show the absence of morphological alterations in a ChAT-positive interneuron adjacent to an Aβ42-ir plaque as well as TH-ir fibers neighboring an APP/Aβ-ir plaque indicated (arrows), respectively. Scale bars in **a**, **d**, **f,** and **i**–**l** = 50 µm and **c**, **e**, **g**, **h** and insets = 10 µm

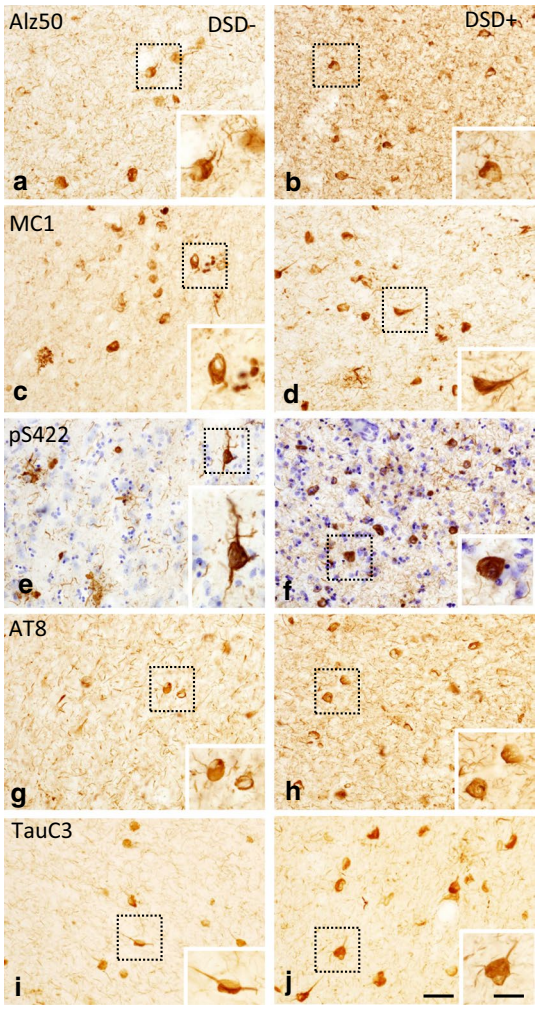

Fig. 4 Photomicrographs showing frontal cortex Alz50 (**a**, **b**), MC1 (**c**, **d**), pS422 (**e**, **f**), AT8 (**g**, **h**), and TauC3 (**i**, **j**)-ir NFTs and NTs in layers V and VI in a 47-year-old female non-demented and a 46-year-old male demented cases with DS. Boxed insets show high-power images of NFTs. Note that all posttranslational Alz50, MC1, pS422, AT8, and TauC3 tau epitopes positive profiles were observed in the frontal cortex in both demented and non-demented cases with DS. pS422-stained section was counterstained with crystal violet (blue) in panels **e** and **f**. 50 µm scale bar in panel **j** also applies images **a**–**i**. The 10 µm scale bar in the **j** inset applies to all insets

(Fig. 3i–l). ChAT-ir neurons adjacent to Aβ42 plaques in the striatum did not show abnormal morphological features (Fig. 3k).

Cortical and striatal NFTs and NTs counts in DSD- and DSD+

To determine whether changes in posttranslational tau epitopes differ in the FC and striatum between DS groups, NFT and NT counts were performed. FC layer V and VI glutamatergic neurons, which are susceptible to NFT pathology, were evaluated [11, 47]. Sections from both

Table 4 Summary of NFT- and NT-positive counts in the frontal cortex by clinical diagnosis

	DSD- ($n=6$)	DSD+ ($n=10$)	p value[a]	Pair-wise comparisons
NFTs				
Alz50	2.70 ± 1.20*	4.10 ± 0.90	0.40	–
MC1	6.50 ± 2.60	10.00 ± 1.80	0.30	–
pS422	10.70 ± 4.30	17.00 ± 2.20	0.30	–
AT8	4.20 ± 1.40	10.00 ± 1.10	0.03	DSD − < DSD+
TauC3	10.00 ± 4.20	17.80 ± 2.30	0.10	–
NTs				
Alz50	118.90 ± 17.60	141.10 ± 5.90	0.20	–
MC1	99.20 ± 30.70	107.00 ± 16.70	1.00	–
pS422	138.00 ± 40.90	209.00 ± 8.10	0.30	–
AT8	117.80 ± 29.10	186.00 ± 11.50	0.03	DSD − < DSD+
TauC3	99.80 ± 37.10	168.80 ± 2.30	0.10	–

*Mean ± standard error

[a]Mann–Whitney rank sum test

regions were processed using tau antibodies pS422, AT8, Alz50, MC1, TauC3, and MN423. In FC, pS422, AT8, Alz50, MC1, and TauC3 positive tau profiles (NFTs and NTs) were observed in layers V and VI in all DSD- and DSD + cases (Fig. 4), except DS case five, which had rare NTs and lacked NFTs (see Table 1). Visual assessment of various tau epitopes revealed that pS422 and the late truncated TauC3 NFTs and NTs were more abundant compared to conformational Alz50 or MC1 profiles in cortical layers V and VI in both DS groups (Fig. 4, Table 4). However, statistical analyses only revealed differences in pS422 and TauC3 compared to Alz50-positive NFT profile densities in the FC of the DSD + group (Fig. 5a, Kruskal–Wallis rank sum test, $p < 0.001$). In addition, pS422 positive NT numbers were significantly higher than MC1- and Alz50-ir NT profiles (Fig. 5b, Kruskal–Wallis rank sum test, $p < 0.001$), and the number of AT8-ir NTs was greater than MC1-ir NTs in DSD +, but not in the DSD − group (Fig. 5b, Kruskal–Wallis rank sum test, $p < 0.05$). Furthermore, NFT counts showed that only the number of FC AT8-ir NFTs and NTs was significantly higher in DSD + compared to DSD − (Table 4 and Fig. 5a, b, Mann–Whitney Rank Sum test, $p < 0.05$). By contrast, MN423 positive profiles were seen in only 2/6 DSD − (33%) compared to 6/8 DSD + (75%) cases. MN423-ir profiles were seen mainly in layers II and III, with the exception of two female cases with DSD + (59 and 45 years old) where NFTs were also observed in layers V and VI (Online Resource 3a, b). Counts of MN423-ir NFTs in FC (layers II, III, and Vl) showed a trend towards higher numbers in DSD + (Online Resource 3c, Mann–Whitney rank sum test, $p = 0.06$).

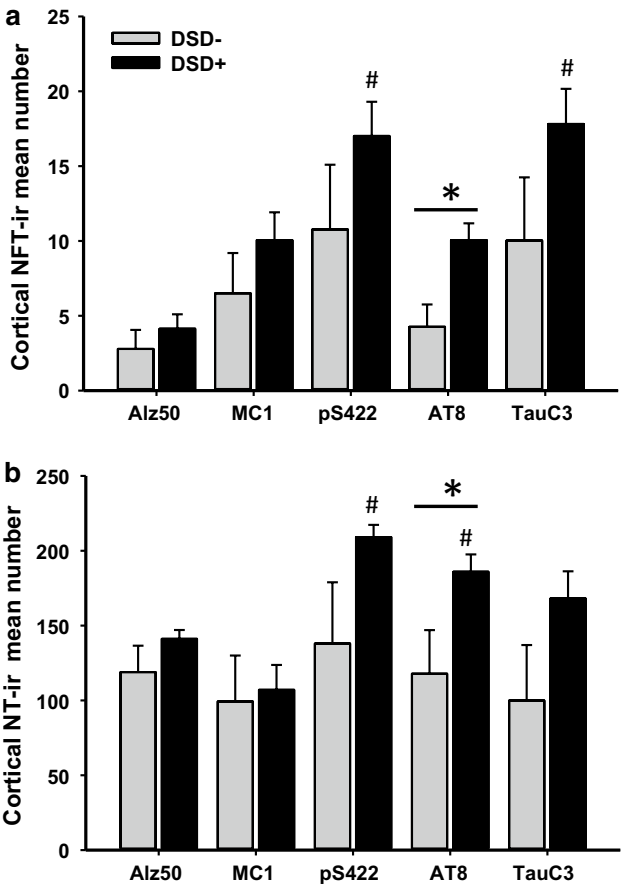

Fig. 5 Histograms showing significant increases in AT8-ir NFTs (**a**) and NTs (**b**) densities in the frontal cortex of demented compared to non-demented subjects with DS (*Mann–Whitney test, $p < 0.05$). Within-group, statistical analysis revealed significantly greater phosphorylated pS422-ir and truncated TauC3-ir NFT densities compared to Alz50-ir NFT density in the frontal cortex in demented (#Kruskal–Wallis test, $p < 0.001$), but not in DS without dementia (**a**). Frontal cortex AT8 and pS422-ir NT numbers were significantly increased compared to conformational MC1-ir NTs in demented (#Kruskal–Wallis test $p < 0.05$), but not in DS without dementia (**b**)

Striatal pS422, AT8, Alz50, MC1, and TauC3-positive NFT profiles were detected in all DSD + cases, whereas conformational Alz50 and MC1-positive NFT profiles were observed in a subset of DSD − cases (Fig. 6a–t). MN423-ir profiles were not detected in the striatum of either DS group (Fig. 6u–x). Quantitation of pS422, AT8, Alz50, MC1, and TauC3-positive striatal NFTs revealed higher numbers of pS422 compared to TauC3-ir NFTs in the putamen compared to caudate (Fig. 7) in DSD − (Fig. 7b, Kruskal–Wallis rank sum test, $p = 0.030$) and DSD + (Fig. 7b, Kruskal–Wallis rank sum test, $p = 0.013$). However, there were no significant differences in pS422, AT8, TauC3, MC1, and Alz50 positive NFTs in the caudate or putamen between DS groups (Table 5 and Fig. 7a, b, Mann–Whitney rank sum test, $p > 0.05$).

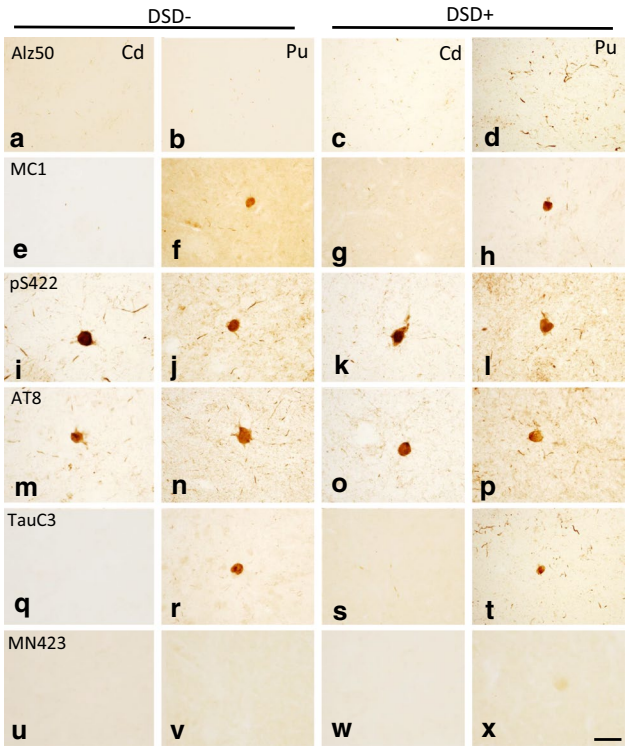

Fig. 6 Photomicrographs showing Alz50 (**a**–**d**), MC1 (**e**–**h**), pS422 (**i**–**l**), AT8 (**m**–**p**), and TauC3 (**q**–**t**)-ir profiles in the caudate and/or putamen in a 60-year-old female non-demented and in a 46-year-old male demented subject with DS. By contrast, MN423-positive profiles were lacking in both regions of the striatum in both demented and non-demented cases with DS (**u**–**x**). Abbreviations: Cd, caudate, Pu, putamen. 50 µm scale bar in **y** applies to all panels

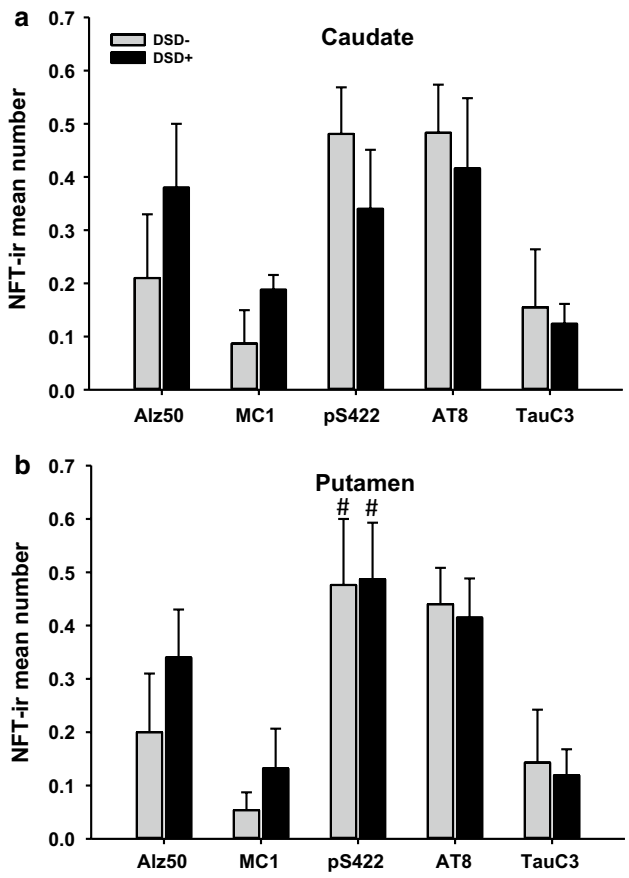

Fig. 7 Histograms showing no differences in pS422, AT8, TauC3, MC1, and Alz50-positive NFT mean numbers either in the **a** caudate or **b** putamen between the two DS groups (Mann–Whitney rank sum test, $p > 0.05$), while pS422-ir NFTs numbers were significantly higher compared to TauC3-ir NFTs in the putamen, but not in the caudate, in demented (#Kruskal–Wallis rank sum test, $p = 0.013$) and non-demented (#Kruskal–Wallis rank sum test, $p = 0.030$) individuals with DS

To characterize the phenotype of the cells displaying tau pathology in the striatum, sections were double immunolabeled using antibodies against AT8 and ChAT in DSD−, DSD+, as well as tissue from an aged non-cognitively impairment (NCI) and sAD subjects (Fig. 8a–i). In the sAD case, ChAT-ir striatal neurons appeared small and rounded compared to AT8 negative perikarya (Fig. 8d–f). By contrast, striatal fusiform-shaped cholinergic neurons (Fig. 8g, i) displayed a normal morphology in DSD- and DSD+ similar to that observed in the NCI case (Fig. 8a, c). However, striatal cholinergic neurons contained aggregations of tau resembling skeins of yarn (Fig. 8h, i), indicating that NFTs develop within striatal aspiny cholinergic interneurons in both DS groups.

Frontal cortex triple immunofluorescence in DSD- and DSD+ cases

To evaluate the evolution of FC layer V and VI NFTs, sections were triple immunolabeled with different combinations of tau antibodies: AT8, pS422, Alz50 and TauC3, pS422, Alz50. Qualitative examination showed that triple-labeled neuron numbers (either AT8 + pS422 + Alz50 or TauC3 + pS422 + Alz50) were greater in DSD+ compared to the DSD− cases (Fig. 9). In addition, the majority of AT8-ir neurons were also pS422 and Alz50 positive. However, not all TauC3-bearing neurons contained pS422 and Alz50 in either DS group (Fig. 9e–h, m–p). Semiquantitative analysis revealed significantly greater numbers of triple AT8 + pS422 + Alz50 (Fig. 10a, Mann–Whitney rank sum test, $p = 0.007$), and double pS422 + Alz50 (Fig. 10a, Mann–Whitney rank sum test, $p = 0.03$) NFTs in DSD+ compared to DSD−. Within-group analysis revealed that the number of cortical NFTs containing AT8 + pS422 + Alz50 was significantly greater than those positive for pS422 + Alz50 in both DS groups (DSD−, Fig. 10a, Friedman RMANOVA, $p < 0.02$; DSD+, Fig. 10a, Friedman RMANOVA, $p = 0.002$), while numbers of NFTs containing AT8 + pS422 + Alz50 were higher than those

Table 5 Summary of NFT-positive counts in caudate and putamen by clinical diagnosis

	DSD- ($n=4$)	DSD+ ($n=4$)	p value[a]	Pair-wise comparisons
Caudate				
Alz50	0.21 ± 0.12*	0.38 ± 0.12	0.70	–
MC1	0.09 ± 0.06	0.19 ± 0.03	0.90	–
pS422	0.50 ± 0.09	0.34 ± 0.11	0.70	–
AT8	0.50 ± 0.09	0.41 ± 0.13	0.70	–
TauC3	0.15 ± 0.10	0.12 ± 0.04	0.70	–
Putamen				
Alz50	0.20 ± 0.11	0.34 ± 0.09	0.50	–
MC1	0.05 ± 0.03	0.13 ± 0.07	0.50	–
pS422	0.50 ± 0.12	0.49 ± 0.10	1.00	–
AT8	0.44 ± 0.07	0.41 ± 0.07	0.90	–
TauC3	0.14 ± 0.12	0.10 ± 0.05	0.70	–

*Mean ± standard error

[a]Mann–Whitney rank sum test

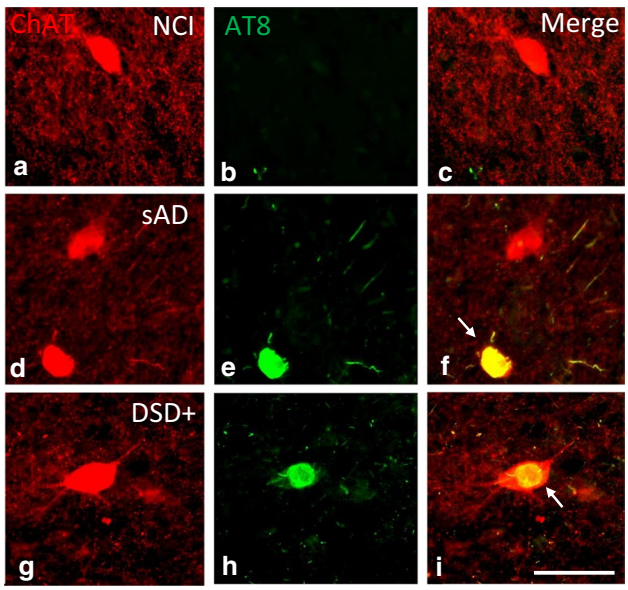

Fig. 8 Immunofluorescence showing striatal neurons single labeled for ChAT (red) and AT8 (green) and merged (yellow) images from a 71-year-old female non-cognitively impaired (**a–c**), a 76-year-old female severe AD (**d–f**) and a 46-year-old male demented DS (**g–i**) case. Note that AT8 NFTs within cholinergic neurons (yellow) in the AD and in demented case with DS, but not in the non-cognitively impaired aged subject. Of particular interest is the globose and shrunken appearance of the cholinergic tangle-bearing neuron (white arrow, **f**) in AD compared to the relative normal morphology despite NFT pathology within cholinergic perikarya in a demented subject with DS (**i**). Abbreviations: NCI, non-cognitive impairment, sAD, severe AD. 50 µm scale bar in **j** applies to all panels

positive for AT8 + Alz50 (Fig. 10a, Friedman RMANOVA, $p=0.007$) in DSD +.

Triple TauC3 + pS422 + Alz50 (Fig. 10b, Mann–Whitney rank sum test, $p=0.02$) and double labeled TauC3 + pS422 (Fig. 10b, Mann–Whitney rank sum test, $p=0.004$) NFTs were significantly greater in DSD + compared to DSD-. Within the DSD + group, numbers of NFTs containing TauC3 + pS422 + Alz50 were higher than both pS422 + Alz50 (Fig. 10b, Friedman RMANOVA, $p<0.001$) and TauC3 + Alz50 (Fig. 10b, Friedman RMANOVA, $p=0.006$) NFTs. Numbers of TauC3 + pS422 positive NFT profiles were significantly greater than pS422 + Alz50 (Fig. 10b, Friedman RMANOVA, $p=0.04$) NFT profiles. No differences were found between double- and triple-labeled NFT numbers in the DSD- group.

Plaque, NFT, and NT correlations

Frontal cortex APP/Aβ and Aβ plaque load (area coverage) and number were strongly correlated within and across groups (Online Resource 4, $r=0.69$–9 $p<0.003$). A strong relationship between cortical X-34 and 6-CN-PiB was also observed (Online Resource 4, $r=0.83$, $p<0.001$) and only X-34 plaque load correlated with TauC3 NFT values (Fig. 11a, $r=0.85$, $p<0.001$, Online Resource 4). Interestingly, APP/Aβ and Aβ plaque load and number were associated with MC1 but not Alz50 positive NT numbers, across groups (Online Resource 4, $r=0.64$–0.73, $p<0.01$). Striatal Aβ plaque load and number strongly correlated with each other (Online Resource 5, $r=0.9$–1, $p<0.001$), but the correlation between APP/Aβ plaque load and APP/Aβ number was not significant (Online Resource 5). X-34 and 6-CN-PiB plaque load in the striatum correlated across DS groups (Online Resource 5, $r=0.93$–0.98, $p<0.001$). Neither histofluorescent amyloid marker correlated with APP/Aβ or Aβ plaque load or number. There were no correlations between FC or striatal plaque pathology, Braak stage, and age across DS groups.

Counts of cortical pS422 NFTs strongly correlated with AT8-bearing neurons (Fig. 11b, $r=0.82$, $p<0.001$, Online Resource 4). The number of Alz50-labeled NFTs was correlated with MC1 containing neurons (Fig. 11c, $r=0.97$, $p<0.001$, Online Resource 4) across groups, respectively, while TauC3 counts showed a weaker relationship with pS422 (Fig. 11d, $r=0.68$, $p=0.004$, Online Resource 4), Alz50 (Online Resource 4, $r=0.60$, $p=0.01$), and MN423 ($r=0.76$, $p=0.001$) NFTs. FC AT8-positive NFT counts correlated with MN423 NFT with and without removal of an outlier (Fig. 11e, $r=0.87$, $p<0.001$, $r=0.59$ $p=0.04$, respectively) and AT8-positive NT number (Fig. 11f, $r=0.85$, $p<0.001$), while pS422 ($r=0.68$, $p=0.003$) and TauC3 (Online Resource 4, $r=0.55$, $p=0.02$) positive NFTs showed a weak correlation with pS422 and TauC3

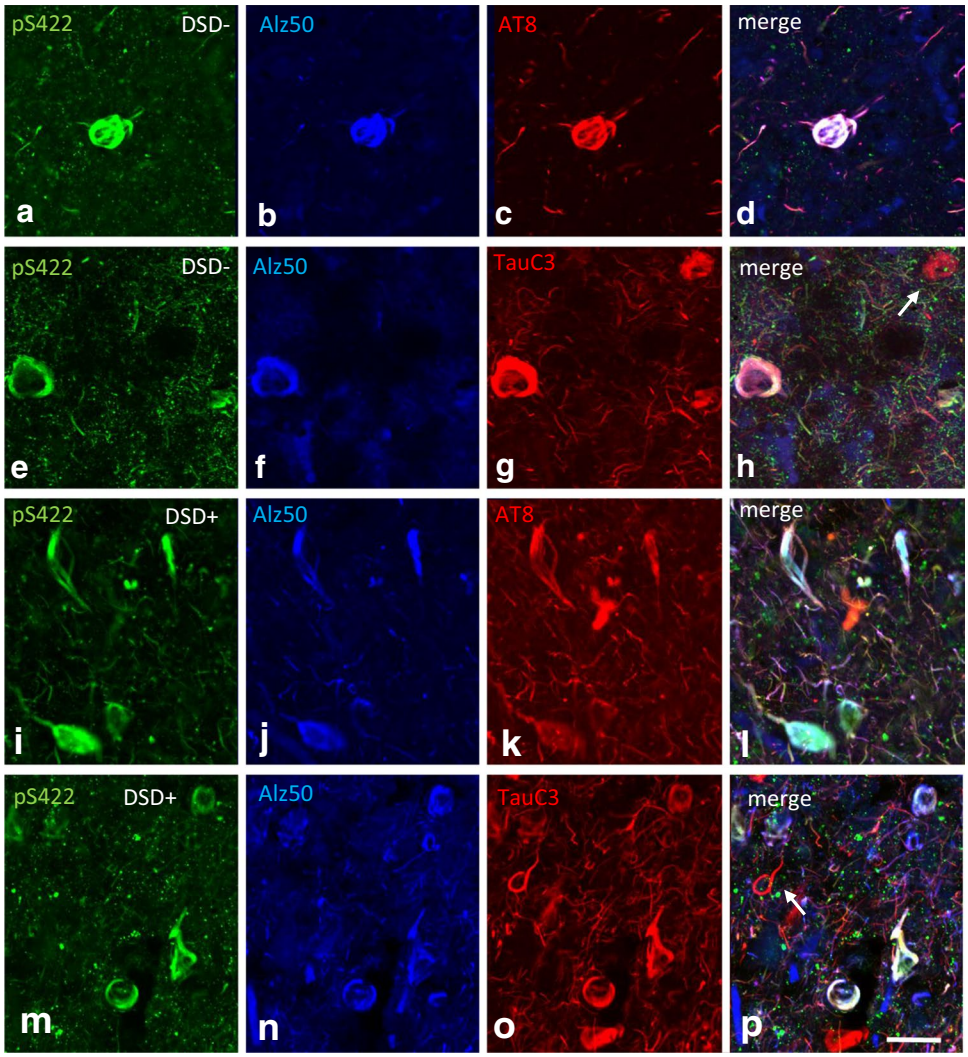

Fig. 9 Confocal immunofluorescence single-labeled images showing pS422 (green) (**a**, **e**, **i, m**), Alz50 (blue) (**b**, **f**, **j**, **n**), AT8 (red) (**c**, **k**) and TauC3 (red) (**g**, **o**) positive profiles and merged images (pink) (**d**, **h**, **l**, **p**) in the frontal cortex of a 44-year-old female non-demented subject with DS (**a**–**h**) and a 46-year-old demented male with DS (**i**–**p**). Note many more cortical pS422 + Alz50 + AT8 and pS422 + Alz50 + TauC3 positive NFTs and NTs (pink) in the demented cases with DS (**l**, **p**) as well as the presence of single cortical TauC3-positive NFTs (white arrow) in both cases (**h**, **p**). 50 µm scale bar in **p** applies to all panels

NT counts, respectively. In addition, pS422 NFT profiles were significantly associated with AT8 NT values ($r = 0.75$, $p < 0.001$) and TauC3 NFTs correlated with pS422 NT ($r = 0.65$, $p = 0.006$) across groups. MC1, pS422, AT8, and TauC3-positive NFTs, but not Alz50, correlated positively with Braak stage ($r = 0.70$, $p = 0.02$). Alz50, AT8, and TauC3-positive NTs correlated positively with Braak stage ($r = 0.60$–0.50, $p = 0.01$–0.03). There were no correlations between FC NFT values and age in either DS group.

AT8 and pS422-positive NFTs correlated with each other in the caudate (Online Resource 6a, pS422 vs AT8 $r = 0.89$, $p = 0.004$) but not in the putamen (Online Resource 6b, pS422 vs AT8 $r = 0.79$, $p = 0.01$), while Alz50 correlated with MC1 positive NFT counts in the putamen (Online Resource 6d, Alz50 vs MC1 $r = 0.95$, $p < 0.001$), but not in the caudate (Online Resource 6c, Alz50 vs MC1 $r = 0.80$, $p > 0.005$) across groups (Online Resource 5). Interestingly, caudate pS422 NFT values displayed a relationship with caudate X-34 plaque load (Online Resource 6e, $r = 0.95$, $p = 0.004$) and 6-CN-PiB (Online Resource 6f, $r = 0.90$, $p = 0.002$), but no putaminal association was found across groups (Online Resource 5).

Frontal cortex expression profiling of pS422 immunopositive neurons

Custom-designed microarrays were used to compare gene expression profiles in FC layers V and VI pS422-ir neurons between DSD − and DSD + groups. Quantitative analysis revealed 64 transcripts related to amyloid and cytoskeleton/tau related biology, glutamatergic, cholinergic and monoaminergic metabolism, endocytosis, and intracellular signaling, which were significantly altered between the two groups (Mann–Whitney rank sum test, $p<0.05$, Online Resource 7–10).

Specifically, transcript levels related to AD markers: APP/Aβ metabolism -β-secretase (*Bace1*), γ-secretase components nicastrin (*Ncstn*), presenilin enhancer 2 (*Psenen*),

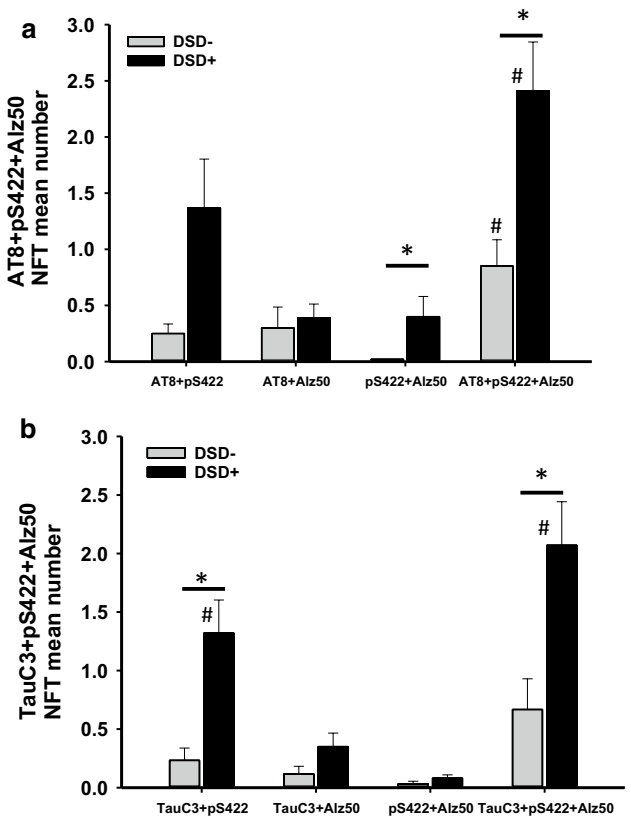

Fig. 10 **a** Histogram showing significantly greater numbers of triple AT8 + pS422 + Alz50 (*Mann–Whitney rank sum test, $p = 0.007$), and double pS422 + Alz50 (*Mann–Whitney rank sum test, $p = 0.03$) positive NFTs in the frontal cortex of demented compared to non-demented individuals with DS. Cortical AT8 + pS422 + Alz50 NFT numbers were significantly higher than pS422 + Alz50 NFT numbers in non-demented (#Friedman RMANOVA, $p < 0.02$) and demented subjects with DS (#Friedman RMANOVA, $p = 0.002$), while AT8 + pS422 + Alz50-positive NFT numbers were greater than AT8 + Alz50 positive NFT number (Friedman RMANOVA, $p = 0.007$) only in demented subjects with DS. **b** Histogram showing a significantly higher number of TauC3 + pS422 + Alz50 (*Mann–Whitney rank sum test, $p = 0.02$) and TauC3 + pS422 (*Friedman RMANOVA test, $p = 0.004$) positive NFTs in demented compared to non-demented DS. Within-group analysis revealed that the number of TauC3 + pS422 + Alz50 NFT was greater than pS422 + Alz50 (#Friedman RMANOVA, $p < 0.001$) and TauC3 + Alz50 (#Friedman RMANOVA, $p = 0.006$) positive NFTs and TauC3 + pS422-positive NFTs were significantly higher than pS422 + Alz50 (#Friedman RMANOVA, $p = 0.04$) NFTs in DS with dementia, while no differences between triple- and double-labeled NFT numbers were observed in non-demented DS

anterior pharynx defective 1A subunit (*Aph1a*), α-secretase ADAM10 component (*Adam10*), and the calcium-binding protein calsenilin (*Kcnip3*), lipoprotein metabolism: very-low-density lipoprotein receptor (*Vldlr*), the apolipoprotein serum amyloid A4 (*Saa4*), and the high-density lipoprotein (*Hdlbp*), tau (*Mapt5*), prion (*Prnp*), and parkin7 (*Park7/Dj1*) were significantly downregulated only in DSD + (Fig. 12a, Online Resource 7). Among AD-related genes (Online Resource 7), *Mapt5* ($r = 0.59$, $p = 0.02$) and *Vldlr* ($r = 0.56$, $p = 0.03$) were correlated moderately with APP/Aβ plaque load; however, these correlations were not significant after adjusting for multiple comparisons (FDR $\alpha = 0.003$). *Aph1a* ($r = -0.54$, $p = 0.04$), *Park7/Dj1* ($r = -$t0.69, $p = 0.005$), *Prnp* ($r = -0.57$, $p = 0.03$), and *Saa4* ($r = -0.52$, $p = 0.05$) were correlated moderately with NTs; however, these correlations were not significant after adjusting for multiple comparisons (FDR $\alpha = 0.002$). No significant correlations were found between the AD-related genes and NFT measures.

The glutamatergic-related neurotransmission markers glutamate receptor 1 (mGluR) 1 (*Grm1*) and 5 (*Grm5*), NMDA receptor subunits 2B (*Grin2b*) and 2D (*Grin2d*), kainate receptor 2 (*Grik2*), AMPA receptor 3 (*Gria3*), excitatory amino acid transporter 1 (*Slc1a3*) and 3 (*Slc1a1*), glutamate receptor interacting protein 1 (*Grip1*) and 2 (*Grip2*), and transglutaminase 1 (*Tgm1*) transcript levels were downregulated in DSD + compared to the DSD − group (Fig. 12b, Online Resource 8). Plaque load and counts, and NFT measures showed no significant correlation with any glutamatergic transcripts. AT8 NT number correlated with Gria3 ($r = -0.59$, $p = 0.02$), Grin2b ($r = -0.52$, $p = 0.05$) and Grin2d ($r = -0.52$, $p = 0.05$), although these correlations were not statistically significant after adjusting for multiple comparisons (FDR $\alpha = 0.002$). Similarly, expression levels of the cholinergic-related neurotransmission markers acetylcholinesterase (*Ache*), butyrylcholinesterase (*Bche*), muscarinic acetylcholine receptor M2 (*Chrm2*) and M4 (*Chmr4*), cholinergic receptor nicotinic alpha 2 (*Chrna2*), 3 (*Chrna3*), 4(*Chrna4*), and 7 (*Chrna7*) subunits, as well as the monoaminergic-related neurotransmission α1B adrenergic receptor (*Adra1b*), serotonin receptor 1B (*Htr1b*), 2C (*Htr2c*), 3A (*Htr3a*), 7 (*Htr7*), monoamine oxidase A (*Maoa*) and B (*Maob*), noradrenaline transporter (*Slc6a2*), serotonin transporter (*Slc6a4*), and tyrosine hydroxylase (*Th*) were downregulated in individuals with DSD + (Fig. 13a, Online Resource 9). Among the monoaminergic genes *Slc6a2* expression correlated with AT8 NTs ($r = -0.54$, $p = 0.04$), but this correlation was not significant after adjusting for multiple comparisons. None of the other genes showed significant correlations with plaques or NFTs prior to multiple comparison adjustment.

Transcript levels of the autoimmune regulator (*Aire*) and FAM3B protein (*Fam3b*), both located on chromosome 21, the *development neocortical-related* empty spiracles homeobox 2 (*Emx2*) transcript factor and the autophagy protein 5 (*Atg5*) were downregulated in DSD + (Fig. 13b, Online Resource 10). Cell survival/death markers including the death-related tumor necrosis factor receptor (TNF) type-1 (*Tradd*), p53 (*Tp53*), caspase 6 (*Casp6*), BCL2-associated X (*Bax*), cell cycle cyclin proteins: cyclin B1 (*Ccnb1*), cyclin D1 (*Ccnd1*) and cyclin D2 (*Ccnd2*), G-proteins: (*Rgs2*),

(*Rgs3*), (*Rgs4*), (*Rgs9*), (*Rgs10*)-, and adenylate cyclase 1 (*Adcy1*) and 6 (*Adcy6*) transcripts were downregulated in DSD+. The proto-oncogene c-fos (*Fos*), Jun (proto-oncogene *Jun*), protein fosB (*Fosb*), and the transcript factor EB (*Tfeb*) were also significantly downregulated in DSD- (Fig. 13b, Online Resource 10). Conversely, the expression levels of the epigenetic gene *Sirt6* were significantly upregulated in DSD+ compared to DSD− (Fig. 13b, Online Resource 10). *Rgs2* expression correlated with APP plaque load ($r=0.53$, $p=0.04$) and counts ($r=0.52$, $p=0.05$), but these correlations were not significant after adjusting for multiple comparisons. None of the other genes showed significant correlations with NFTs or NTs prior to multiple comparison adjustment.

Table 6 shows no significant differences in transcript levels associated with DS pathogenic genes located on chromosome 21 including amyloid precursor protein (*App*), Down syndrome critical region 1 (*Dscr1*), dual-specificity, and tyrosine phosphorylation-regulated kinase1A (*Dyrk1A*), as well in other randomly chosen genes non-located on chromosome HSA21 including caveolin 2 (Cav2), drebrin (*Dbn1*), doublecourtin (*Dcx*), apolipoprotein E (*Apoe*), sirtuin 3 (*Sirt3*), and alpha synuclein (*Snca*) (Online Resource 11, Mann Mann–Whitney rank sum test, $p>0.05$). *Dscr1* correlated with X-34 plaque load ($r=0.54$, $p=0.04$), while *Dyrk1a* correlated with APP plaque load ($r=-0.64$, $p=0.02$) and counts ($r=-0.57$, $p=0.03$). However, these correlations were not significant after multiple comparison adjustment. None of the other genes showed significant correlations with NFTs or NTs prior to multiple comparison adjustment.

Immunohistochemical gene-array validation

Immunolabeling of the *Sirt6* gene product was performed to validate our single-cell gene-array findings. We found that nuclear SIRT6 immunoreactivity was stronger in cells of cortical layers V and VI in DSD+ compared to DSD− cases (Online Resource 12), confirming the upregulation *Sirt6* observed on the custom-designed array platform in DSD+.

Discussion

Frontal cortex and striatal plaque pathology in DSD− and DSD+

Plaque severity was determined by measuring plaque load (area) and plaque numbers. Interestingly, differences in cortical and striatal APP/Aβ (6E10), Aβ (MOAB2), X-34, and 6-CN-PiB positive plaque load as well as APP/Aβ and Aβ positive plaque numbers were not detected between DSD+ and DSD- cases. By contrast, FC APP/Aβ and X-34-labeled plaque load was significantly higher compared to Aβ and 6-CN-PiB plaque loads, respectively, but not in the striatum in the DSD+ group, suggesting that APP and non-fibrillar Aβ contribute to a greater degree to cortical plaque pathology in DSD+. In addition, the number of striatal APP/Aβ-positive plaques was significantly higher than those reactive for Aβ compared to the FC in DSD− cases. In this regard, FC plaques showed intense X-34 and 6-CN-PiB fluorescence in DSD+ and DSD− and displayed features indicative of cored/neuritic plaques [121], similar to a previous study showing strong ^{3}H-PiB and 6-CN-PiB binding in the FC of adult individuals with DS [70], demonstrating the fibrillar nature of Aβ in the FC of those with DS. On the other hand, striatal plaques showed weak X-34 and 6-CN-PiB fluorescence and lacked a central core [121] indicative of more dispersed and less densely packed Aβ fibrils, characteristic of diffuse plaques [49, 50, 59]. These observation are consistent with autopsy [50, 98] and in vivo PET imaging studies using [11C]PiB in DS [4, 44, 45, 64–66, 130], familial [61, 62, 85, 109, 111, 116, 132], and sporadic AD [51, 58, 60, 115]. Swollen dystrophic neurites positive for neurofilament and MC1 were associated with Aβ42 containing FC plaques, but not in the striatum, supporting our observation of neuritic plaques in the former but diffuse in the latter in both DSD− and DSD+ [47, 77] similar to AD [27]. Furthermore, striatal cholinergic or dopaminergic dystrophic neurites were not found in association with amyloid plaques or within the striatal neuropil. It is particularly interesting that striatal cholinergic interneurons contained NFT pathology, but their morphology remained similar to that seen in the aged cognitively normal case examined. These findings question the concept of tau and amyloid toxicity [133], at least in the striatum.

The relationship between amyloid pathology and cognitive impairment in DS is unclear. Hartley and colleagues [45] did not find an association between high levels of neocortical PiB-amyloid retention in adults with DS with or without dementia. By contrast, high plasma Aβ and tau levels were associated with demented individuals with DS [67, 117, 119], while others showed no differences in plasma Aβ levels in adults with DS with or without dementia [56]. However, fibrillar Aβ PiB in vivo imaging showed ligand retention first in the striatum and then the cortex in DS [4, 44, 64, 130], similar to what has been reported in familial AD (FAD) [61]. In addition, higher PiB retention correlated with cognitive decline and dementia in DS [4]. Although PET imaging indicates that the early and high striatal amyloid pathology seen in DS are reminiscent of that observed in FAD [13, 44], higher striatal PiB retention in FAD was not associated with cognitive status [132]. The observation that striatal PiB binding precedes cortical labeling suggests more advanced fibrillar Aβ deposits in people with DS [4,

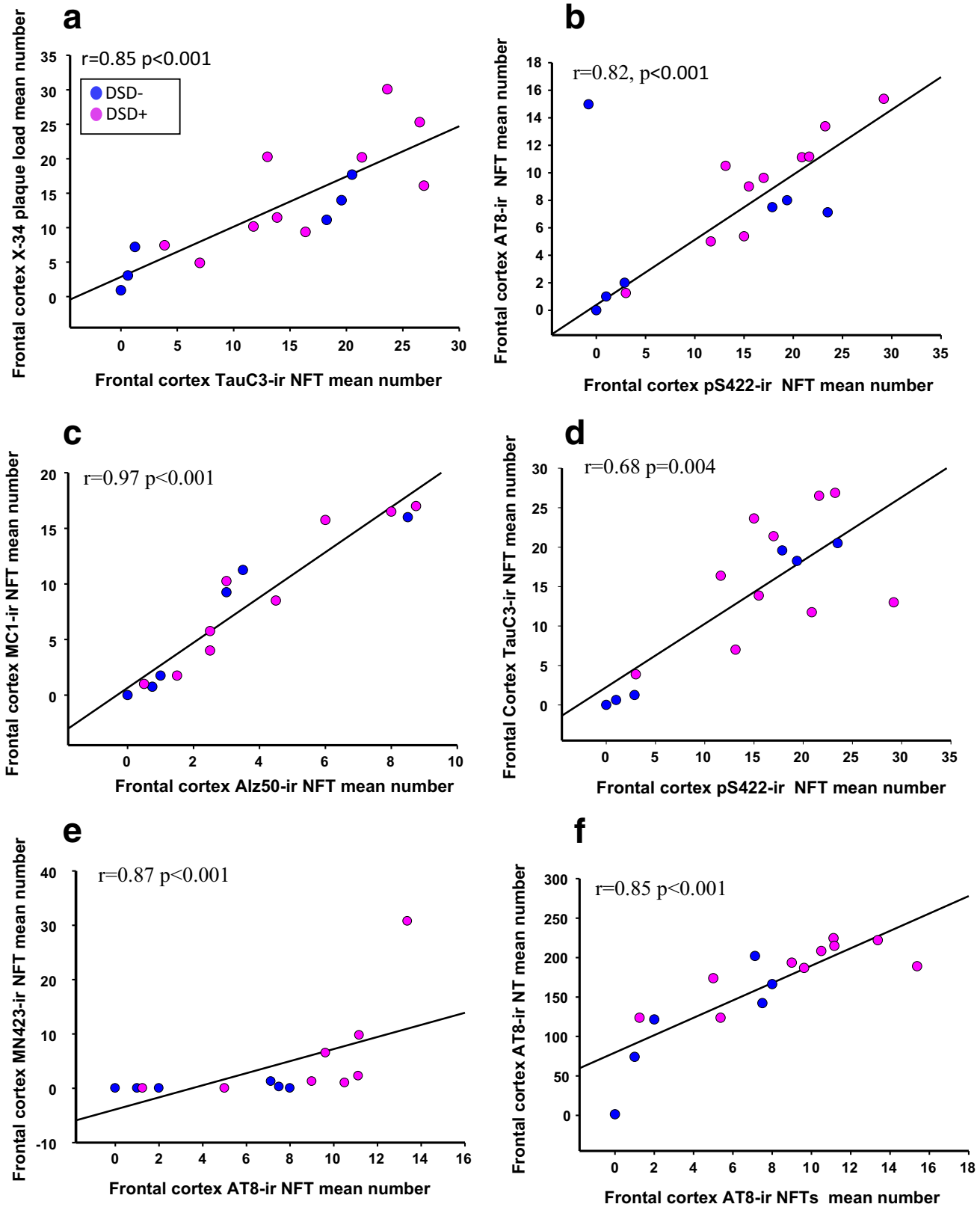
a
r=0.85 p<0.001
DSD-
DSD+
Frontal cortex X-34 plaque load mean number
Frontal cortex TauC3-ir NFT mean number
b
r=0.82, p<0.001
Frontal cortex AT8-ir NFT mean number
Frontal cortex pS422-ir NFT mean number
c
r=0.97 p<0.001
Frontal cortex MC1-ir NFT mean number
Frontal cortex Alz50-ir NFT mean number
d
r=0.68 p=0.004
Frontal Cortex TauC3-ir NFT mean number
Frontal cortex pS422-ir NFT mean number
e
r=0.87 p<0.001
Frontal cortex MN423-ir NFT mean number
Frontal cortex AT8-ir NFT mean number
f
r=0.85 p<0.001
Frontal cortex AT8-ir NT mean number
Frontal cortex AT8-ir NFTs mean number

◂**Fig. 11** Linear regression graphs showing a strong significant positive correlation between frontal cortex X-34 plaque load and TauC3 NFTs values (**a**, $r=0.85$, $p<0.001$), cortical pS422 and Alz50 NFT counts, and phosphorylated AT8 (**b**, $r=0.82$, $p<0.001$), and MC1 (**c**, $r=0.97$, $p<0.001$) across the groups, while TauC3 counts showed a weaker relationship with pS422 (**d**, $r=0.68$, $p=0.004$). Cortical phosphorylated AT8-positive NFT counts were strongly associated with the number of MN423-bearing NFTs (**e**, $r=0.87$, $p<0.001$) and AT8 (**f**, $r=0.85$, $p<0.001$) positive NT numbers

44, 64]. However, plaque pathology was recently reported to originate in the neocortex followed by subcortical areas, including the striatum in postmortem DS tissue [18]. Further investigations comparing PiB imaging with immunohistochemical plaque staining are needed to resolve this discrepancy. Overall, FC and striatal plaque load and number were similar between DSD + and DSD − groups, suggesting that other aspects of neurodegeneration after 40 years of age, such as neuritic dystrophy and/or tau pathology, play a more critical role in the onset of dementia in adults with DS. Alternatively, the early onset of Aβ accumulation prior to NFT formation suggests a dual-hit scenario.

Frontal cortex and striatal tangle pathology in DSD- and DSD+

AT8 was the only posttranscriptional epitope showing differences between DS groups. In this regard, FC AT8 positive NFT and NT counts were significantly higher in DSD + compared to DSD-. In FC, AT8 co-localized with Alz50, pS422, and TauC3 in NFT and the number of AT8-ir NFTs correlated with pS422 and MN423-ir NFTs. Unlike pS422, which marks phosphorylation at the C-terminal domain [125], AT8 detects phosphorylated amino acids in the middle, proline-rich region of the tau epitope [38] and is associated with a more severe stage of AD [1]. We also found that AT8 and pS422 positive NTs were higher than those displaying tau conformational changes in DSD +, suggesting that phosphorylated tau epitopes are an early pathogenic events associated with cognitive deficits in DS similar to AD [104, 131]. Since tau is involved in the regulation of motor proteins that play a key role in cellular cargo transport, accumulations of tau in neuronal processes have been related to axonal transport deficits [57] in the early stages of abnormal tau formation [133], resulting in synaptic loss and cognitive impairment in DS. In fact, pS422 immunoreactivity in cholinergic neurons in the nucleus basalis of Meynert was correlated with cognitive decline in AD progression [131]. pS422, which co-localizes with oligomeric tau [102, 129, 133], inhibits anterograde and retrograde fast axonal transport in AD [129]. Therefore, the larger number of FC phosphorylated NTs in DSD + suggests that phosphorylation of tau contributes to axonal transport deficits in DSD +.

Surprisingly, the majority of pS422 immunoreactivity reported here was associated with fibrillar tau in the FC and striatum in both DS groups indicating an advanced stage of tau aggregation. In addition, higher numbers of FC pS422 NFTs containing Alz50/AT8, and Alz50/TauC3 epitopes were observed in DSD + than in DSD-, most likely reflecting a more widespread cortical tau pathology in DSD +, where phosphorylated tau co-localized with conformational and late truncated tau events to a greater degree. Remarkably, in vivo and in vitro studies suggest that tau phosphorylation at Serine^{422} prevents truncation at the C-terminal by caspase 3 [22, 40, 113] significantly delaying events related to the interaction between phospho-Serine^{422} and truncation Aspartic^{421} (D^{421}) in AD [40]. However, we found numerous cortical NFT profiles that displayed both TauC3 and pS422 in DSD + cases, suggesting that these posttranslational events occur close in time, perhaps, associated with an upregulation of Down syndrome critical region 1 (DSCR1) [23, 123] and tyrosine phosphorylation-regulated kinase1 (DYRK1) [72, 134] protein levels associated with tau phosphorylation in DS. The greater number of NFTs displaying Serine^{422} in FC and striatum suggests that phosphorylation of tau at this site is an early event in tau pathogenesis in DS [19, 21, 48]. In fact, blood levels of exosomal phosphorylated Serine^{396} tau were reported to be significantly higher in DSD+ compared to those DSD- [43] reflecting widespread tau phosphorylation in the brain of DSD +. The density of TauC3 positive NFT profiles was significantly higher than conformational Alz50 containing tangles within the FC in DSD + cases. The TauC3 epitope is associated with a more mature NFTs, detecting cleavage of tau at the Aspartic^{421} site by the apoptotic enzyme caspase 3, mainly in fibrillar tau structures [25, 110] after the appearance of tau phosphorylation epitopes [90, 91], and contemporary to the conformational Alz50, which herald the appearance of filamentous/fibrillar tau in NFTs in AD [41]. By contrast, we found lower numbers of Alz50 positive FC NFTs, suggesting a later occurrence than tau truncation. Here, we found that cortical numbers of NFTs containing Alz50 + pS422 and Alz50 + TauC3 epitopes were lower compared to AT8 + pS422 + Alz50 and TauC3 + pS422 + Alz50 NFTs in DSD- and DSD +, respectively, suggesting that phosphorylation and truncation precede conformational tau events in DS supporting an alternative model of tangle maturation in AD (Mondragon-Rodriguez et al. [90]). By contrast, putaminal TauC3 NFT density was significantly lower than pS422, but comparable to Alz50 in both DS groups, revealing a less advanced stage of NFT maturation, where phosphorylation at Serine^{422} precedes cleavage at D^{421} and conformational changes detected by Alz50. Interestingly, TauC3 was reported in soluble misfolded tau "propagation seeds" in AD, suggesting a role for truncation at D^{421} early in the

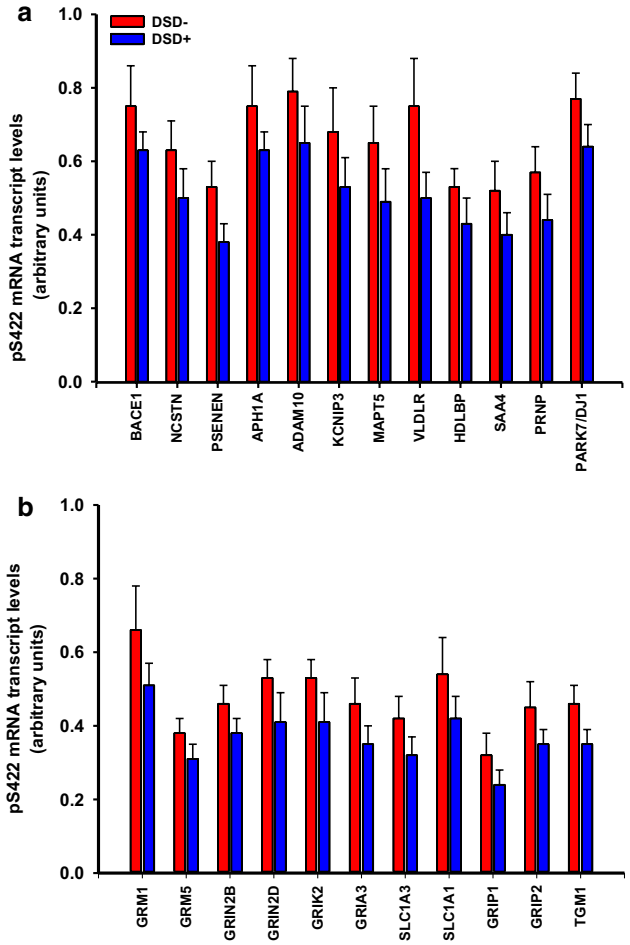

Fig. 12 Histograms showing a downregulation in the mean values of relative signal intensity of mRNA transcripts related to (**a**) APP/Aβ metabolism [β-secretase (*Bace)*, γ-secretase (*Ncstn*, *Psenen, Aph1a*), α-secretase (*Adam10*) and calsenilin (*Kcnip3*)], lipoprotein metabolism (*Vldlr*, *Saa, Hdlbp*), tau (*Mapt5*), prion (*Prnp*), parkin7 (*Park7/Dj1*) and (**b**) glutamatergic neurotransmission [mGluR1 (*Grm1*) and 5 (mGluR5) (*Grm5*) receptors, NMDA receptor subunits 2B (*Grin2b*) and 2D (*Grin2d*), Glutamate receptor ionotropic, kainate 2 (*Grik2*), AMPA ionotropic glutamate receptor 3 (*Gria3*), transporters 1 (*Slc1a3*) and 3 (*Slc1a1*), glutamate receptor interacting protein 1 (*Grip1*) and 2 (*Grip2*), and transglutaminase 1 (*Tgm1*)] derived from single frontal cortex pS422 positive NFTs in demented compared to non-demented subjects with DS (Mann–Whitney rank sum test, $p < 0.05$)

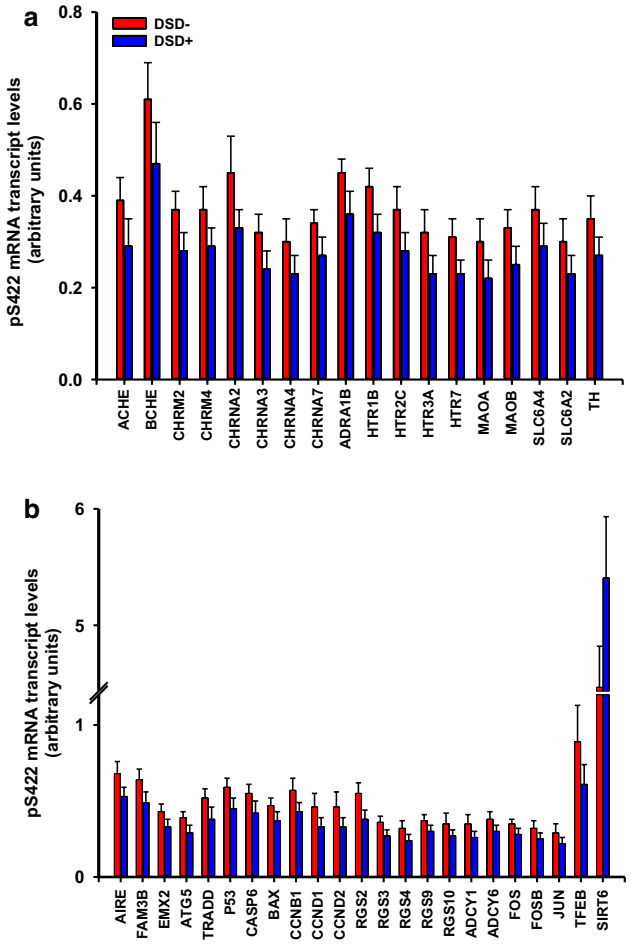

Fig. 13 **a** Histogram showing downregulation of expression levels of several cholinergic [acetylcholinesterase (*Ache*), butyrylcholinesterase (*Bche*), muscarinic receptor M2 (*Chrm2*), M4 (*Chmr4*), cholinergic receptor nicotinic alpha 2 (*Chrna2*), 3 (*Chrna3*), 4 (*Chrna4*) and 7 (*Chrna7*) subunits], and monoaminergic [α1B adrenergic receptor (*Adra1b*), serotonin receptor 1B (*Htr1b*), 2C (*Htr2c*), 3A (*Htr3a*), 7 (*Htr7*), monoamine oxidase A (*Maoa*) and B (*Maob*), noradrenaline transporter (*Slc6a2*), serotonin transporter (*Slc6a4*) and tyrosine hydroxylase (*Th*)] neurotransmission-related genes in frontal cortex pS422 positive NFTs in demented compared to non-demented subjects with DS (Mann–Whitney rank sum test, $p < 0.05$). **b** Histogram showing downregulation of autoimmune regulator (*Aire*), FAM3B protein (*Fam3b*), homeobox 2 (*Emx2*) transcript factor, the autophagy protein 5 (*Atg5*), TNF type-1 (*Tradd*), protein p53 (*Tp53*), caspase 6 (*Casp6*), BCL2-associated X (*Bax*), several cyclin proteins [cyclin B1 (*Ccnb1*), cyclin D1 (*Ccnd1*) and cyclin D2 (*Ccnd2*)], G-proteins [(*Rgs2*), (*Rgs3*), (*Rgs4*), (*Rgs9*), (*Rgs10*)], adenylate cyclases [(*Adcy1*), (*Adcy6*)], proto-oncogene c-fos (*Fos*), Jun (*Jun*), protein fosB (*Fosb*), and transcript factor EB (*Tfeb*) mRNAs in frontal cortex pS422-positive NFTs in demented compared to non-demented subjects with DS, while transcript expression levels for the *Sirt6* gene were upregulated in frontal cortex pS422-positive NFTs in demented compared to non-demented subjects with DS (Mann–Whitney rank sum test, $p < 0.05$)

evolution of NFT pathology in AD [99] that could explain the greater number of TauC3 NFTs in DS.

Gene profiling in cortical pS422 tangle-bearing neurons in DSD – and DSD+

Single-population expression profiling of cortical pS422 tangle-bearing neurons revealed significant alterations in 64 transcripts examined related to amyloid/tau biology, glutamatergic, cholinergic and monoaminergic metabolism,

Table 6 Example of stable gene transcripts in FC pS422 neurons between DSD− and DSD+

Gene abbreviation	Group	Gene/protein name	DSD- ($n=5$)	DSD+ ($n=10$)	Comparison** (p value)	Function
APP	AD	Amyloid-β precursor protein	0.60 ± 0.10*	0.50 ± 0.07	ns	APP/Aβ metabolism
APOE	GLIA	Apolipoprotein-E	0.49 ± 0.06	0.41 ± 0.05	ns	Cholesterol metabolism
CAV2	CYT	Caveolin 2	2.14 ± 0.60	2.92 ± 0.50	ns	Cellular homeostasis
SNCA	SYN	Alpha synuclein	1.21 ± 0.30	1.24 ± 0.16	ns	Synapsis
DSCR1	DS	DS critical region protein 1	0.52 ± 0.50	0.05 ± 0.07	ns	Cell homeostasis
DYRK1A	PP/K	Dual-specificity tyrosine phosphorylation-regulated kinase1A	1.90 ± 0.30	2.20 ± 0.30	ns	Cell proliferation
DBN1	DV	Drebrin 1	0.43 ± 0.07	0.35 ± 0.06	ns	Synapsis
DCX	DV	Doublecortin	0.48 ± 0.06	0.41 ± 0.05	ns	Cell proliferation
SIRT3	SIRT	Sirtuin 3	0.80 ± 0.40	0.60 ± 0.20	ns	Gene regulation

AD Alzheimer's disease, *GLIA* glia-associated markers, *CYT* cytoskeletal elements, *DS* Down syndrome, *PP/K* protein phosphatases and kinases, *DV* development-related markers, *SIRT* sirtuin proteins, *ns* non-significant

*Mean ± standard deviation

**Mann–Whitney with false discovery rate-adjusted p value

intracellular signaling, and cell homeostasis between DSD+ and DSD− subjects. Reduction in the APP amylodogenic (e.g., β-secretase and γ-secretase-associated transcripts and non-amylodogenic pathways (e.g., α-secretase) in DSD+, while *App* was unchanged between groups, consistent with previous observations in the adult DS brain and fetal fibroblasts [6, 73]. The lack of differential regulation in the FC of *App* in DS is consistent with our observations in cholinergic basal forebrain [33, 94], CA1 pyramidal neurons [30, 35] in AD, and pS422-bearing cholinergic neurons in chronic traumatic encephalopathy [95]. We found that the expression levels of the cholesterol carrier *Apoe*, which is involved in Aβ production via α-secretase regulation [122], were comparable between DS groups, while *Apoe* gene expression upregulation was seen in the prefrontal cortex between DS and controls [73]. Cholesterol-related genes *Vldlr*, *Hdlbp,* and *Saa4* were downregulated in DSD+, suggesting that low cholesterol neuronal uptake might favor an APP non-amyloidogenic pathway that may result in APP protein augmentation, which is supported by our findings showing an increase in APP plaque burden in the FC in DSD+.

Gene profiling of FC layer V and VI neurons indicated dysfunction of select genes in other relevant pathways including glutamatergic, cholinergic, and monoaminergic neurotransmission in DSD+, suggesting that a dysregulation of these systems plays a role in cortical dysfunction in demented individuals with DS [20]. Cortical pyramidal glutamatergic neuron excitability is modulated via metabotropic muscarinic and ionotropic nicotinic receptors by acetylcholine [107], a neurotransmitter synthesized in cholinergic basal forebrain neurons within the nucleus basalis of Meynert [86, 88], which display deficits in DS [80, 82, 136]. Gene expression levels of *Ache* [87], the acetylcholine degrading enzyme, were also downregulated in DSD+. In addition, transcripts related to monoaminergic and serotonergic receptors, which interact with FC pyramidal neurons [3, 89, 114], were also downregulated in DSD+. Noradrenergic and serotoninergic cortical innervation arises from neurons located within the locus coeruleus [55, 101] and raphe nuclei [14, 100], respectively, which contain NFTs in adults with DS [16, 18, 79, 82], suggesting that alterations in extraneuronal cortical projections systems affect FC neuron expression in DSD+.

Evidence for dysregulation of genes related to the immune system and cell cycle was found in DS. For example, *Aire*, which plays a crucial role in autoimmunity, is diminished in the thymus in DS [29] and was downregulated in DSD+. Several other immune-related genes were upregulated in DS compared to controls [73], supporting immune system deficits in DS patients. We also found a reduction in cell death/cell cycle/proliferation related genes within cortical NFTs in DSD+, which has shown to be upregulated in prefrontal cortex brain homogenates of adults with DS compared to controls [73]. Moreover, gene and protein levels of the epigenetic marker *Sirt6*, a nuclear deacetylase enzyme involved in DNA repair, tumor suppression, and oxidative stress [71, 74, 120], were increased in DSD+. Taken together, these data suggest that genes related to cellular homeostasis are dysfunctional in NFT-bearing FC neurons in DSD+.

There are caveats associated with this study that merit discussion. For example, there are a limited number of postmortem DS cases available, especially clinically well-characterized DS subjects. In particular, the relatively small number of striatal cases evaluated in the present study advised for a conservative interpretation of these data.

Moreover, inadequate record keeping, profound intellectual disability, or lack of proper cognitive testing can be a pitfall associated with DS studies. In this regard, only UIC and BSHRI cases received extensive premortem cognitive testing. For the Rush cases, an individual's physician and interviews with family members determined the diagnosis of dementia. The later could lead to an incorrect clinical diagnosis. Despite these caveats, we found that the genomic and histopathological findings' was sufficient for an experimenter blinded to case antemortem diagnosis to place each subject in its appropriate clinical category. These findings suggest that combining vulnerable single population genetic and neuropathological characteristics could provide a biomarker for DSD+. In addition, frozen brain tissue from the individuals with DS examined was not available for qPCR validation of expression data or determination of RNA integrity. However, we were able to confirm profiling findings for *Sirt6* using immunocytochemistry of tissue from the same cases used for the genetic signature analysis. The lack of large numbers of antemortem well-characterized clinical and postmortem neuropathological evaluated DS cases supports the need to stress brain banking from individuals with DS at all ages.

In summary, we found a greater number and more advanced NFTs in FC, but not in the striatum in DSD+, while Aβ load in both cortical and subcortical regions was comparable between groups. The density of cortical NFTs and NTs positive for the pretangle marker pS422 and the late truncated TauC3 epitopes were upregulated compared to conformational tau events in DSD+. Likewise, cortical pretangle bearing FC pS422 neurons exhibited a select downregulation of classes of transcripts related to amyloid/tau biology, glutamatergic, cholinergic, and monoaminergic neurotransmission, intracellular signaling, and cell homeostasis in DSD+. The profile of vulnerable FC pyramidal layer V and VI neurons between DSD− and DSD+, suggests that these two groups have similarities as well as differences in neuropathological and gene expression signatures that may be used to develop therapeutic interventions that arrest cognitive decline in this population that represents a unique genetic model of early AD.

Acknowledgements We gratefully acknowledge the contribution of Ms. L. Shao and Mr. M. Nadeem. This work was supported by the National Institute of Health (grants: P01 AG025204 and R01 AG052528 to M.D.I, R01 AG061566 to E.J.M., PPG AG014449 to E.J.M., S.D.G. and M.D.I, R01 AG043375 to S.D.G. and E.J.M., and P01 AG017617 to S.D.G.), Bright Focus Foundation (E.J.M.), and by the Arizona Alzheimer's Consortium at Barrow Neurological Institute (S.E.P.).

Author contributions Study concept and design: SEP and EJM. Acquisition of data: SEP, JM, EA, MM-A and BH. Analysis and interpretation of data: SEP and EJM. Drafting of the article: SEP and EJM. Critical revision of the article for important intellectual content: MDI, EA, IL, ED, SDG, and MJA. Facilitation of access to DS tissue: IL and ED. Study supervision: EJM.

Compliance with ethical standards

Ethical responsibilities All authors had full access to all the data in the study and take responsibility for the integrity of the data and the accuracy of the data analysis. The authors declared that the manuscript has not been submitted to other journal for publication or has been published previously partly or in full. The authors report no conflict of interest.

References

1. Alafuzoff I, Arzberger T, Al-Sarraj S, Bodi I, Bogdanovic N, Braak H et al (2008) Staging of neurofibrillary pathology in Alzheimer's disease: a study of the BrainNet Europe Consortium. Brain Pathol 18:484–496
2. Alldred MJ, Che S, Ginsberg SD (2009) Terminal continuation (TC) RNA amplification without second strand synthesis. J Neurosci Methods 177:381–385
3. Amargós-Bosch M, Bortolozzi A, Puig MV, Serrats J, Adell A, Celada P et al (2004) Co-expression and in vivo interaction of serotonin1A and serotonin2A receptors in pyramidal neurons of prefrontal cortex. Cereb Cortex 14:281–299
4. Annus T, Wilson LR, Hong YT, Acosta-Cabronero J, Fryer TD, Cardenas-Blanco A et al (2016) The pattern of amyloid accumulation in the brains of adults with Down syndrome. Alzheimers Dement 12:538–545
5. Arendt T, Stieler JT, Holzer M (2016) Tau and tauopathies. Brain Res Bull 126:238–292
6. Argellati F, Massone S, d'Abramo C, Marinari UM, Pronzato MA, Domenicotti C (2006) Evidence against the overexpression of APP in Down syndrome. IUBMB Life 58:103–106
7. Arnold SE, Hyman BT, Flory J, Damasio AR, Van Hoesen GW (1991) The topographical and neuroanatomical distribution of neurofibrillary tangles and neuritic plaques in the cerebral cortex of patients with Alzheimer's disease. Cereb Cortex 1:103–116
8. Bakkar RM, Luo G, Webb TA, Crutcher KA, de Courten-Myers GM (2010) Down's syndrome with Alzheimer's disease-like pathology: what can it teach us about the amyloid cascade hypothesis? Int J Alzheimers Dis. https://doi.org/10.4061/2010/175818
9. Basurto-Islas G, Luna-Muñoz J, Guillozet-Bongaarts AL, Binder LI, Mena R, García-Sierra F (2008) Accumulation of aspartic acid421- and glutamic acid391-cleaved tau in neurofibrillary tangles correlates with progression in Alzheimer disease. J Neuropathol Exp Neurol 67:470–483
10. Braak H, Braak E (1991) Neuropathological stageing of Alzheimer-related changes. Acta Neuropathol 82:239–259
11. Braak H, Rüb U, Schultz C, Del Tredici K (2006) Vulnerability of cortical neurons to Alzheimer's and Parkinson's diseases. J Alzheimers Dis 9:35–44
12. Che S, Ginsberg SD (2004) Amplification of RNA transcripts using terminal continuation. Lab Invest 84:131–137
13. Cohen AD, McDade E, Christian B, Price J, Mathis C, Klunk W et al (2018) Early striatal amyloid deposition distinguishes Down syndrome and autosomal dominant Alzheimer's disease from late-onset amyloid deposition. Alzheimers Dement 14:743–750

14. Conrad LC, Leonard CM, Pfaff DW (1974) Connections of the median and dorsal raphe nuclei in the rat: an autoradiographic and degeneration study. J Comp Neurol 156:179–205
15. Counts SE, Alldred MJ, Che S, Ginsberg SD, Mufson EJ (2014) Synaptic gene dysregulation within hippocampal CA1 pyramidal neurons in mild cognitive impairment. Neuropharmacology 79:172–179
16. Counts SE, He B, Che S, Ikonomovic MD, DeKosky ST, Ginsberg SD et al (2007) Alpha7 nicotinic receptor up-regulation in cholinergic basal forebrain neurons in Alzheimer disease. Arch Neurol 64:1771–1776
17. Counts SE, Mufson EJ (2010) Noradrenaline activation of neurotrophic pathways protects against neuronal amyloid toxicity. J Neurochem 113:649–660
18. Davidson YS, Robinson A, Prasher VP, Mann DMA (2018) The age of onset and evolution of Braak tangle stage and Thal amyloid pathology of Alzheimer's disease in individuals with Down syndrome. Acta Neuropathol Commun 6:56
19. de Calignon A, Polydoro M, Suárez-Calvet M, William C, Adamowicz DH, Kopeikina KJ et al (2012) Propagation of tau pathology in a model of early Alzheimer's disease. Neuron 73:685–697
20. Dekker AD, Vermeiren Y, Carmona-Iragui M, Benejam B, Videla L, Gelpi E et al (2017) Monoaminergic impairment in Down syndrome with Alzheimer's disease compared to early-onset Alzheimer's disease. Alzheimers Dement 10:99–111
21. DeVos SL, Corjuc BT, Oakley DH, Nobuhara CK, Bannon RN, Chase A et al (2018) Synaptic tau seeding precedes tau pathology in human Alzheimer's Disease brain. Front Neurosci 12:267
22. Flores-Rodríguez P, Ontiveros-Torres MA, Cárdenas-Aguayo MC, Luna-Arias JP, Meraz-Ríos MA, Viramontes-Pintos A et al (2015) The relationship between truncation and phosphorylation at the C-terminus of tau protein in the paired helical filaments of Alzheimer's disease. Front Neurosci 9:33
23. Fuentes JJ, Genescà L, Kingsbury TJ, Cunningham KW, Pérez-Riba M, Estivill X et al (2000) DSCR1, overexpressed in Down syndrome, is an inhibitor of calcineurin-mediated signaling pathways. Hum Mol Genet 9:1681–1690
24. Galvin JE, Ginsberg SD (2004) Expression profiling and pharmacotherapeutic development in the central nervous system. Alzheimer Dis Assoc Disord 18:264–269
25. Gamblin TC, Chen F, Zambrano A, Abraha A, Lagalwar S, Guillozet AL et al (2003) Caspase cleavage of tau: linking amyloid and neurofibrillary tangles in Alzheimer's disease. Proc Natl Acad Sci USA 100:10032–10037
26. García-Sierra F, Ghoshal N, Quinn B, Berry RW, Binder LI (2003) Conformational changes and truncation of tau protein during tangle evolution in Alzheimer's disease. J Alzheimers Dis 5:65–77
27. Gearing M, Levey AI, Mirra SS (1997) Diffuse plaques in the striatum in Alzheimer disease (AD): relationship to the striatal mosaic and selected neuropeptide markers. J Neuropathol Exp Neurol 56:1363–1370
28. Ghoshal N, García-Sierra F, Fu Y, Beckett LA, Mufson EJ, Kuret J et al (2001) Tau-66: evidence for a novel tau conformation in Alzheimer's disease. J Neurochem 77:1372–1385
29. Giménez-Barcons M, Casteràs A, del Armengol M, Porta EP, Correa PA, Marín A et al (2014) Autoimmune predisposition in Down syndrome may result from a partial central tolerance failure due to insufficient intrathymic expression of AIRE and peripheral antigens. J Immunol 193:3872–3879
30. Ginsberg SD, Alldred MJ, Counts SE, Cataldo AM, Neve RL, Jiang Y et al (2010) Microarray analysis of hippocampal CA1 neurons implicates early endosomal dysfunction during Alzheimer's disease progression. Biol Psychiatry 68:885–893
31. Ginsberg SD, Che S (2004) Combined histochemical staining, RNA amplification, regional, and single cell cDNA analysis within the hippocampus. Lab Invest 84:952–962
32. Ginsberg SD, Che S, Counts SE, Mufson EJ (2006) Single cell gene expression profiling in Alzheimer's disease. NeuroRx 3:302–318
33. Ginsberg SD, Wuu CS, Counts JSE, Mufson EJ (2006) Down regulation of trk but not p75NTR gene expression in single cholinergic basal forebrain neurons mark the progression of Alzheimer's disease. J Neurochem 97:475–487
34. Ginsberg SD, Elarova I, Ruben M, Tan F, Counts SE, Eberwine JH et al (2004) Single-cell gene expression analysis: implications for neurodegenerative and neuropsychiatric disorders. Neurochem Res 29:1053–1064
35. Ginsberg SD, Hemby SE, Lee VM, Eberwine JH, Trojanowski JQ (2000) Expression profile of transcripts in Alzheimer's disease tangle-bearing CA1 neurons. Ann Neurol 48:77–87
36. Ginsberg SD, Malek-Ahmadi MH, Alldred MJ, Che S, Elarova I, Chen Y et al (2017) Selective decline of neurotrophin and neurotrophin receptor genes within CA1 pyramidal neurons and hippocampus proper: correlation with cognitive performance and neuropathology in mild cognitive impairment and Alzheimer's disease. Hippocampus. https://doi.org/10.1002/hipo.22802
37. Glasson EJ, Sullivan SG, Hussain R, Petterson BA, Montgomery PD, Bittles AH (2002) The changing survival profile of people with Down's syndrome: implications for genetic counselling. Clin Genet 62:390–393
38. Goedert M, Jakes R, Vanmechelen E (1995) Monoclonal antibody AT8 recognises tau protein phosphorylated at both serine 202 and threonine 205. Neurosci Lett 189:167–169
39. Guedj F, Pennings JL, Massingham LJ, Wick HC, Siegel AE, Tantravahi U et al (2016) An integrated human/murine transcriptome and pathway approach to identify prenatal treatments for Down syndrome. Sci Rep. https://www.nature.com/articles/srep32353
40. Guillozet-Bongaarts AL, Cahill ME, Cryns VL, Reynolds MR, Berry RW, Binder LI (2006) Pseudophosphorylation of tau at serine 422 inhibits caspase cleavage: in vitro evidence and implications for tangle formation in vivo. J Neurochem 97:1005–10014
41. Guillozet-Bongaarts AL, Garcia-Sierra F, Reynolds MR, Horowitz PM, Fu Y, Wang T et al (2005) Tau truncation during neurofibrillary tangle evolution in Alzheimer's disease. Neurobiol Aging 26:1015–1022
42. Gyure KA, Durham R, Stewart WF, Smialek JE, Troncoso JC (2001) Intraneuronal abeta-amyloid precedes development of amyloid plaques in Down syndrome. Arch Pathol Lab Med 125:489–492
43. Hamlett ED, Goetzl EJ, Ledreux A, Vasilevko V, Boger HA, LaRosa A et al (2017) Neuronal exosomes reveal Alzheimer's disease biomarkers in Down syndrome. Alzheimers Dement 13:541–549
44. Handen BL, Cohen AD, Channamalappa U, Bulova P, Cannon SA, Cohen WI et al (2012) Imaging brain amyloid in nondemented young adults with Down syndrome using Pittsburgh compound B. Alzheimers Dement 8:496–501
45. Hartley SL, Handen BL, Devenny DA, Hardison R, Mihaila I, Price JC et al (2014) Cognitive functioning in relation to brain amyloid-β in healthy adults with Down syndrome. Brain 137:2556–2563
46. Head E, Lott IT, Wilcock DM, Lemere CA (2016) Aging in Down syndrome and the development of Alzheimer's disease neuropathology. Curr Alzheimer Res 13:18–29
47. Hof PR, Bouras C, Perl DP, Sparks DL, Mehta N, Morrison JH (1995) Age-related distribution of neuropathologic changes in the cerebral cortex of patients with Down's syndrome. Quantitative

regional analysis and comparison with Alzheimer's disease. Arch Neurol 52:379–391
48. Hu W, Zhang X, Tung YC, Xie S, Liu F, Iqbal K (2016) Hyperphosphorylation determines both the spread and the morphology of tau pathology. Alzheimers Dement 12:1066–1077
49. Ikonomovic MD, Abrahamson EE, Isanski BA, Debnath ML, Mathis CA, Dekosky ST et al (2006) X-34 labeling of abnormal protein aggregates during the progression of Alzheimer's disease. Methods Enzymol 412:123–144
50. Ikonomovic MD, Klunk WE, Abrahamson EE, Mathis CA, Price JC, Tsopelas ND et al (2008) Post-mortem correlates of in vivo PiB-PET amyloid imaging in a typical case of Alzheimer's disease. Brain 131:1630–1645
51. Ishibashi K, Ishiwata K, Toyohara J, Murayama S, Ishii K (2014) Regional analysis of striatal and cortical amyloid deposition in patients with Alzheimer's disease. Eur J Neurosci 40:2701–2706
52. Iulita MF, Do Carmo S, Ower AK, Fortress AM, Flores Aguilar L, Hanna M et al (2014) Nerve growth factor metabolic dysfunction in Down's syndrome brains. Brain 137:860–872
53. Iulita MF, Ower A, Barone C, Pentz R, Gubert P, Romano C et al (2016) An inflammatory and trophic disconnect biomarker profile revealed in Down syndrome plasma: relation to cognitive decline and longitudinal evaluation. Alzheimers Dement 12:1132–1148
54. Jennings D, Seibyl J, Sabbagh M, Lai F, Hopkins W, Bullich S (2015) Age dependence of brain β-amyloid deposition in Down syndrome: an [18F]florbetaben PET study. Neurology 84:500–507
55. Jones BE, Moore RY (1977) Ascending projections of the locus coeruleus in the rat. II autoradiographic study. Brain Res 127:25–53
56. Jones EL, Hanney M, Francis PT, Ballard CG (2009) Amyloid beta concentrations in older people with Down syndrome and dementia. Neurosci Lett 451:162–164
57. Kanaan NM, Morfini GA, LaPointe NE, Pigino GF, Patterson KR, Song Y et al (2011) Pathogenic forms of tau inhibit kinesin-dependent axonal transport through a mechanism involving activation of axonal phosphotransferases. J Neurosci 31:9858–9868
58. Kemppainen NM, Aalto S, Wilson IA, Någren K, Helin S, Brück A et al (2006) Voxel-based analysis of PET amyloid ligand [11C] PIB uptake in Alzheimer disease. Neurology 67:1575–1580
59. Kida E, Choi-Miura NH, Wisniewski KE (1995) Deposition of apolipoproteins E and J in senile plaques is topographically determined in both Alzheimer's disease and Down's syndrome brain. Brain Res 685:211–216
60. Klunk WE, Engler H, Nordberg A, Wang Y, Blomqvist G, Holt DP et al (2004) Imaging brain amyloid in Alzheimer's disease with Pittsburgh compound-B. Ann Neurol 55:306–319
61. Klunk WE, Price JC, Mathis CA, Tsopelas ND, Lopresti BJ, Ziolko SK et al (2007) Amyloid deposition begins in the striatum of presenilin-1 mutation carriers from two unrelated pedigrees. J Neurosci 27:6174–6184
62. Koivunen J, Verkkoniemi A, Aalto S, Paetau A, Ahonen JP, Viitanen M et al (2008) PET amyloid ligand [11C]PIB uptake shows predominantly striatal increase in variant Alzheimer's disease. Brain 131:1845–1853
63. Landt J, D'Abrera JC, Holland AJ, Aigbirhio FI, Fryer TD, Canales R et al (2011) Using positron emission tomography and Carbon 11-labeled Pittsburgh compound B to image brain fibrillar β-amyloid in adults with down syndrome: safety, acceptability, and feasibility. Arch Neurol 68:890–896
64. Lao PJ, Betthauser TJ, Hillmer AT, Price JC, Klunk WE, Mihaila I et al (2016) The effects of normal aging on amyloid-β deposition in nondemented adults with Down syndrome as imaged by carbon 11-labeled Pittsburgh compound B. Alzheimers Dement 12:380–390
65. Lao PJ, Handen BL, Betthauser TJ, Mihaila I, Hartley SL, Cohen AD et al (2017) Longitudinal changes in amyloid positron emission tomography and volumetric magnetic resonance imaging in the nondemented Down syndrome population. Alzheimers Dement (Amst) 9:1–9
66. Lao PJ, Handen BL, Betthauser TJ, Mihaila I, Hartley SL, Cohen AD et al (2018) Alzheimer-like pattern of hypometabolism emerges with elevated amyloid-β burden in Down syndrome. J Alzheimers Dis 61:631–644
67. Lee NC, Yang SY, Chieh JJ, Huang PT, Chang LM, Chiu YN et al (2017) Blood beta-amyloid and tau in Down syndrome: a comparison with Alzheimer's disease. Front Aging Neurosci. https://doi.org/10.3389/fnagi.2016.00316
68. Lemere CA, Blusztajn JK, Yamaguchi H, Wisniewski T, Saido TC, Selkoe DJ (1996) Sequence of deposition of heterogeneous amyloid beta-peptides and APOE in Down syndrome: implications for initial events in amyloid plaque formation. Neurobiol Dis 3:16–32
69. Leverenz JB, Raskind MA (1998) Early amyloid deposition in the medial temporal lobe of young Down syndrome patients: a regional quantitative analysis. Exp Neurol 150:296–304
70. LeVine H 3rd, Spielmann HP, Matveev S, Cauvi FM, Murphy MP, Beckett TL et al (2017) Down syndrome: age-dependence of PiB binding in postmortem frontal cortex across the lifespan. Neurobiol Aging 54:163–169
71. Liao CY, Kennedy BK (2016) SIRT6, oxidative stress, and aging. Cell Res 26:143–144
72. Liu F, Liang Z, Wegiel J, Hwang YW, Iqbal K, Grundke-Iqbal I et al (2008) Overexpression of Dyrk1A contributes to neurofibrillary degeneration in Down syndrome. FASEB J 22:3224–3233
73. Lockstone HE, Harris LW, Swatton JE, Wayland MT, Holland AJ, Bahn S (2007) Gene expression profiling in the adult Down syndrome brain. Genomics 90:647–660
74. Lombard DB (2009) Sirtuins at the breaking point: sIRT6 in DNA repair. Aging 1:12–16
75. Mahady L, Nadeem M, Malek-Ahmadi M, Chen K, Perez SE et al (2018) HDAC2 dysregulation in the nucleus basalis of Meynert during the progression of Alzheimer's disease. Neuropathol Appl Neurobiol 45:122. https://doi.org/10.1111/nan.12518
76. Mann DM, Esiri MM (1989) The pattern of acquisition of plaques and tangles in the brains of patients under 50 years of age with Down's syndrome. J Neurol Sci 89:169–179
77. Mann DM, Iwatsubo T (1996) Diffuse plaques in the cerebellum and corpus striatum in Down's syndrome contain amyloid beta protein (A beta) only in the form of A beta 42(43). Neurodegeneration 5:115–120
78. Mann DM, Prinja D, Davies CA, Ihara Y, Delacourte A, Défossez A et al (1989) Immunocytochemical profile of neurofibrillary tangles in Down's syndrome patients of different ages. J Neurol Sci 92:247–260
79. Mann DM, Yates PO, Hawkes J (1983) The pathology of the human locus ceruleus. Clin Neuropathol 2:1–7
80. Mann DM, Yates PO, Marcyniuk B (1984) Alzheimer's presenile dementia, senile dementia of Alzheimer type and Down's syndrome in middle age form an age related continuum of pathological changes. Neuropathol Appl Neurobiol 10:185–207
81. Mann DM, Yates PO, Marcyniuk B, Ravindra CR (1986) The topography of plaques and tangles in Down's syndrome patients of different ages. Neuropathol Appl Neurobiol 12:447–457
82. Mann DM, Yates PO, Marcyniuk B, Ravindra CR (1987) Loss of neurones from cortical and subcortical areas in Down's syndrome patients at middle age. Quantitative comparisons with younger Down's patients and patients with Alzheimer's disease. J Neurol Sci 80:79–89

83. Margallo-Lana ML, Moore PB, Kay DW, Perry RH, Reid BE, Berney TP et al (2007) Fifteen-year follow-up of 92 hospitalized adults with Down's syndrome: incidence of cognitive decline, its relationship to age and neuropathology. J Intellect Disabil Res 51:463–477
84. Matthews DC, Lukic AS, Andrews RD, Marendic B, Brewer J, Rissman RA et al (2016) Dissociation of Down syndrome and Alzheimer's disease effects with imaging. Alzheimers Dement (N Y) 2:69–81
85. McDade E, Kim A, James J, Sheu LK, Kuan DC, Minhas D et al (2014) Cerebral perfusion alterations and cerebral amyloid in autosomal dominant Alzheimer disease. Neurology 83:710–717
86. Mesulam MM (2013) Cholinergic circuitry of the human nucleus basalis and its fate in Alzheimer's disease. J Comp Neurol 521:4124–4144
87. Mesulam MM, Geula C (1991) Acetylcholinesterase-rich neurons of the human cerebral cortex: cytoarchitectonic and ontogenetic patterns of distribution. J Comp Neurol 306:193–220
88. Mesulam MM, Mufson EJ, Levey AI, Wainer BH (1983) Cholinergic innervation of cortex by the basal forebrain: cytochemistry and cortical connections of the septal area, diagonal band nuclei, nucleus basalis (substantia innominata), and hypothalamus in the rhesus monkey. J Comp Neurol 214:170–197
89. Miner LA, Backstrom JR, Sanders-Bush E, Sesack SR (2003) Ultrastructural localization of serotonin2A receptors in the middle layers of the rat prelimbic prefrontal cortex. Neuroscience 116:107–117
90. Mondragón-Rodríguez S, Basurto-Islas G, Santa-Maria I, Mena R, Binder LI, Avila J et al (2008) Cleavage and conformational changes of tau protein follow phosphorylation during Alzheimer's disease. Int J Exp Pathol 89:81–90
91. Mondragón-Rodríguez S, Mena R, Binder LI, Smith MA, Perry G, García-Sierra F (2008) Conformational changes and cleavage of tau in Pick bodies parallel the early processing of tau found in Alzheimer pathology. Neuropathol Appl Neurobiol 34:62–75
92. Mondragón-Rodríguez S, Perry G, Luna-Muñoz J, Acevedo-Aquino MC, Williams S (2014) Phosphorylation of tau protein at sites Ser(396-404) is one of the earliest events in Alzheimer's disease and Down syndrome. Neuro Appl Neurobiol 40:121–135
93. Motte J, Williams RS (1989) Age-related changes in the density and morphology of plaques and neurofibrillary tangles in Down syndrome brain. Acta Neuropathol 77:535–546
94. Mufson EJ, Counts SE, Ginsberg SD (2002) Gene expression profiles of cholinergic nucleus basalis neurons in Alzheimer's disease. Neurochem Res 27:1035–1048
95. Mufson EJ, He B, Ginsberg SD, Carper BA, Bieler GS, Crawford F et al (2018) Gene profiling of nucleus basalis tau containing neurons in chronic traumatic encephalopathy: a chronic effects of neurotrauma consortium study. J Neurotrauma 35:1260–1271
96. Mufson EJ, Perez SE, Nadeem M, Mahady L, Kanaan NM, Abrahamson EE et al (2016) Progression of tau pathology within cholinergic nucleus basalis neurons in chronic traumatic encephalopathy: a chronic effects of neurotrauma consortium study. Brain Inj 30:1399–1413
97. Nelson PT, Alafuzoff I, Bigio EH, Bouras C, Braak H, Cairns NJ et al (2012) Correlation of Alzheimer disease neuropathologic changes with cognitive status: a review of the literature. J Neuropathol Exp Neurol 71:362–381
98. Ni R, Gillberg PG, Bogdanovic N, Viitanen M, Myllykangas L, Nennesmo I (2017) Amyloid tracers binding sites in autosomal dominant and sporadic Alzheimer's disease. Alzheimers Dement 13:419–430
99. Nicholls SB, DeVos SL, Commins C, Nobuhara C, Bennett RE, Corjuc DL et al (2017) Characterization of TauC3 antibody and demonstration of its potential to block tau propagation. PLoS One 12:e0177914
100. O'Hearn E, Molliver ME (1984) Organization of raphe-cortical projections in rat: a quantitative retrograde study. Brain Res Bull 13:709–726
101. Olson L, Fuxe K (1971) On the projections from the locus coeruleus noradrenaline neurons: the cerebellar innervation. Brain Res 28:165–171
102. Patterson KR, Remmers C, Fu Y, Brooker S, Kanaan NM, Vana L et al (2011) Characterization of prefibrillar Tau oligomers in vitro and in Alzheimer disease. J Biol Chem 286:23063–23076
103. Perez SE, Getova DP, He B, Counts SE, Geula C, Desire L et al (2012) Rac1b increases with progressive tau pathology within cholinergic nucleus basalis neurons in Alzheimer's disease. Am J Pathol 180:526–540
104. Perez SE, He B, Nadeem M, Wuu J, Scheff SW, Abrahamson EE et al (2015) Resilience of precuneus neurotrophic signaling pathways despite amyloid pathology in prodromal Alzheimer's disease. Biol Psychiatry 77:693–703
105. Perez SE, Raghanti MA, Hof PR, Kramer L, Ikonomovic MD, Lacor PN et al (2013) Alzheimer's disease pathology in the neocortex and hippocampus of the western lowland gorilla (Gorilla gorilla gorilla). J Comp Neurol 521:4318–4338
106. Perez SE, Sherwood CC, Cranfield MR, Erwin JM, Mudakikwa A, Hof PR et al (2016) Early Alzheimer's disease-type pathology in the frontal cortex of wild mountain gorillas (Gorilla beringei beringei). Neurobiol Aging 39:195–201
107. Picciotto MR, Higley MJ, Mineur YS (2012) Acetylcholine as a neuromodulator: cholinergic signaling shapes nervous system function and behavior. Neuron 76:116–129
108. Rafii MS, Lukic AS, Andrews RD, Brewer J, Rissman RA, Strother SC et al (2017) Down Syndrome biomarker initiative and the Alzheimer's disease neuroimaging initiative. PET Imaging of tau pathology and relationship to amyloid, longitudinal MRI, and cognitive change in Down syndrome: results from the Down syndrome biomarker initiative (DSBI). J Alzheimers Dis 60:439–450
109. Remes AM, Laru L, Tuominen H, Aalto S, Kemppainen N, Mononen H et al (2008) Carbon 11-labeled Pittsburgh compound B positron emission tomographic amyloid imaging in patients with APP locus duplication. Arch Neurol 65:540–544
110. Rissman RA, Poon WW, Blurton-Jones M, Oddo S, Torp R, Vitek MP et al (2004) Caspase-cleavage of tau is an early event in Alzheimer disease tangle pathology. J Clin Invest 114:121–130
111. Rodriguez-Vieitez E, Saint-Aubert L, Carter SF, Almkvist O, Farid K, Schöll M et al (2016) Diverging longitudinal changes in astrocytosis and amyloid PET in autosomal dominant Alzheimer's disease. Brain 139:922–936
112. Sabbagh MN, Chen K, Rogers J, Fleisher AS, Liebsack C, Bandy D et al (2015) Florbetapir PET, FDG PET, and MRI in Down syndrome individuals with and without Alzheimer's dementia. JAMA Neurol 72:571–581
113. Sandhu P, Naeem MM, Lu C, Kumarathasan P, Gomes J, Basak A (2017) Ser422 phosphorylation blocks human Tau cleavage by caspase-3: biochemical implications to Alzheimer's disease. Bioorg Med Chem Lett 27:642–652
114. Santana N, Artigas F (2017) Laminar and cellular distribution of monoamine receptors in rat medial prefrontal cortex. Front Neuroanat 11:87
115. Sauerbeck J, Ishii K, Hosokawa C, Kaida H, Scheiwein FT, Hanaoka K et al (2018) The correlation between striatal and cortical binding ratio of 11C-PiB-PET in amyloid-uptake-positive patients. Ann Nucl Med 32:398–403
116. Schöll M, Wall A, Thordardottir S, Ferreira D, Bogdanovic N, Långström B et al (2012) Low PiB PET retention in presence of pathologic CSF biomarkers in Arctic APP mutation carriers. Neurology 79:229–236

117. Schupf N, Patel B, Silverman W, Zigman WB, Zhong N, Tycko B et al (2001) Elevated plasma amyloid β-peptide 1–42 and onset of dementia in adults with Down syndrome. Neurosci Lett 301:199–203
118. Schupf N, Sergievsky GH (2002) Genetic and host factors for dementia in Down's syndrome. Br J Psychiatry 180:405–410
119. Schupf N, Zigman WB, Tang MX, Pang D, Mayeux R, Mehta P et al (2010) Change in plasma Aβ peptides and onset of dementia in adults with Down syndrome. Neurology 75:1639–1644
120. Sebastián C, Zwaans BM, Silberman DM, Gymrek M, Goren A, Zhong L et al (2012) The histone deacetylase SIRT6 is a tumor suppressor that controls cancer metabolism. Cell 151:1185–1199
121. Serrano-Pozo A, Frosch MP, Masliah E, Hyman BT (2011) Neuropathological alterations in Alzheimer disease. Cold Spring Harb Perspect Med 1:a006189
122. Shackleton B, Crawford F, Bachmeier C (2017) Apolipoprotein E-mediated Modulation of ADAM10 in Alzheimer's disease. Curr Alzheimer Res 14:1578–1585
123. Shaw JL, Zhang S, Chang KT (2015) Bidirectional regulation of amyloid precursor protein-induced memory defects by nebula/DSCR1: a protein upregulated in Alzheimer's disease and Down syndrome. J Neurosci 35:11374–11383
124. Sheehan R, Sinai A, Bass N, Blatchford P, Bohnen I, Bonell S et al (2015) Dementia diagnostic criteria in Down syndrome. Int J Geriatr Psychiatry 30:857–863
125. Sontag E, Nunbhakdi-Craig V, Lee G, Brandt R, Kamibayashi C, Kuret J et al (1999) Molecular interactions among protein phosphatase 2A, tau, and microtubules. Implications for the regulation of tau phosphorylation and the development of tauopathies. J Biol Chem 274:25490–25498
126. Styren SD, Hamilton RL, Styren GC, Klunk WE (2000) X-34, a fluorescent derivative of congo red: a novel histochemical stain for Alzheimer's disease pathology. J Histochem Cytochem 48:1223–1232
127. Teller JK, Russo C, DeBusk LM, Angelini G, Zaccheo D, Dagna-Bricarelli F et al (1996) Presence of soluble amyloid beta-peptide precedes amyloid plaque formation in Down's syndrome. Nat Med 2:93–95
128. Tiernan CT, Ginsberg SD, Guillozet-Bongaarts AL, Ward SM, He B, Kanaan NM et al (2016) Protein homeostasis gene dysregulation in pretangle-bearing nucleus basalis neurons during the progression of Alzheimer's disease. Neurobiol Aging 42:80–90
129. Tiernan CT, Mufson EJ, Kanaan NM, Counts SE (2018) Tau oligomer pathology in nucleus basalis neurons during the progression of Alzheimer disease. J Neuropathol Exp Neurol 77:246–259
130. Tudorascu DL, Anderson SJ, Minhas DS, Yu Z, Comer D, Lao P et al (2019) Comparison of longitudinal Aβ in nondemented elderly and Down syndrome. Neurobiol Aging 73:171–176
131. Vana L, Kanaan NM, Ugwu IC, Wuu J, Mufson EJ, Binder LI (2011) Progression of tau pathology in cholinergic Basal forebrain neurons in mild cognitive impairment and Alzheimer's disease. Am J Pathol 179:2533–2550
132. Villemagne VL, Ataka S, Mizuno T, Brooks WS, Wada Y, Kondo M et al (2009) High striatal amyloid beta-peptide deposition across different autosomal Alzheimer disease mutation types. Arch Neurol 66:1537–1544
133. Ward SM, Himmelstein DS, Lancia JK, Binder LI (2012) Tau oligomers and tau toxicity in neurodegenerative disease. Biochem Soc Trans 40:667–671
134. Wegiel J, Dowjat K, Kaczmarski W, Kuchna I, Nowicki K, Frackowiak J et al (2008) The role of overexpressed DYRK1A protein in the early onset of neurofibrillary degeneration in Down syndrome. Acta Neuropathol 116:391–407
135. Wisniewski KE, Wisniewski HM, Wen GY (1985) Occurrence of neuropathological changes and dementia of Alzheimer's disease in Down's syndrome. Ann Neurol 17:278–282
136. Yates CM, Simpson J, Maloney AF, Gordon A, Reid AH (1980) Alzheimer-like cholinergic deficiency in Down syndrome. Lancet 2:979
137. Zigman WB, Devenny DA, Krinsky-McHale SJ, Jenkins EC, Urv TK, Weigel J et al (2008) Alzheimer's disease in adults with Down Syndrome. Int Rev Res Ment Retard 36:103–145
138. Zigman WB, Lott IT (2007) Alzheimer's disease in Down syndrome: neurobiology and risk. Ment Retard Dev Disabil Res Rev 13:237–246
139. Zigman WB, Schupf N, Urv T, Zigman A, Silverman W (2002) Incidence and temporal patterns of adaptive behavior change in adults with mental retardation. Am J Ment Retard 107:161–174